Moffett James (Orcid ID: 0000-0002-2359-8899)
Saito Mak (Orcid ID: 0000-0001-6040-9295)

Efficient zinc/cobalt interreplacement in northeast Pacific diatoms and relationship to high surface dissolved Co:Zn ratios

Marissa M. Kellogg[1], Matthew R. McIlvin[2], Jagruti Vedamati[3], Benjamin S. Twining[4], James W. Moffett[3], Adrian Marchetti[5], Dawn M. Moran[2], Mak A. Saito[2]

[1]MIT/WHOI Joint Program in Oceanography/Applied Ocean Science and Engineering, Woods Hole MA, USA, mkell0gg@mit.edu.

[2]Department of Marine Chemistry and Geochemistry, Woods Hole Oceanographic Institution, Woods Hole MA, USA, mmcilvin@whoi.edu, dmoran@whoi.edu, msaito@whoi.edu.

[3]Department of Biological Sciences, University of Southern California, Los Angeles CA, USA, jvedamati@usc.edu, jmoffett@usc.edu.

[4]Bigelow Laboratory for Ocean Sciences, East Boothbay ME, USA, btwining@bigelow.org.

[5]Department of Marine Sciences, University of North Carolina at Chapel Hill, Chapel Hill NC, USA, amarchet@email.unc.edu.

Corresponding author:

Mak Saito

266 Woods Hole Road, Woods Hole MA 02543

Watson Building 123, MS #51

Office: +1 508 289 2393

msaito@whoi.edu

Running heading: Use of Zn and Co in northeast Pacific diatoms

Abstract

The importance of zinc (Zn) as a nutrient and its ability to be substituted for by cobalt (Co) have been characterized in model marine diatoms. However, the extent to which this substitution capability is distributed among diatom taxa is unknown. Zn/Co metabolic substitution was assayed in four diatom species as measured by the effect of free ion concentrations of Zn^{2+} and Co^{2+} on specific growth rate. Analysis of growth responses found substitution of these metals can occur within the northwest Atlantic isolate *Thalassiosira pseudonana* CCMP1335, the northeast Atlantic isolate *Phaeodactylum tricornutum* CCMP632, and within the northeast Pacific isolates *Pseudo-nitzschia delicatissima* UNC1205 and *Thalassiosira sp.* UNC1203. Metabolic substitution of Co in place of Zn in the Atlantic diatoms supports their growth in media lacking added Zn, but at the cost of reduced growth rates. In contrast, highly efficient Zn/Co substitution that supported growth even in media lacking added Zn was observed in the northeast Pacific diatoms. Diatom growth rate responses were compared to total dissolved concentrations of Zn and Co measured in the surface ocean of their native environments. New data from the northeast Pacific Line P transect reveals dissolved Co and Zn ratios (dCo:dZn) as high as 3.52:1 at surface (0 – 100 m) depths, which is unusual given the much larger deep inventory of Zn. To our knowledge the measured dCo:dZn ratios of Line P are the first observations of dCo abundance exceeding dZn. We posit that the enhanced ability of the NE Pacific diatoms to grow using Co is an adaptation to the high surface dCo:dZn ratios present

there. Particulate metal data and analysis of single-cell metal quotas from the Line P transect both indicate that a high Zn demand exists in diatoms that may be partially compensated for by Co.

Introduction

Marine diatoms are photosynthetic microorganisms prevalent throughout the oceans that are estimated to contribute up to 20% of global primary productivity (Armbrust 2009). In eukaryotes such as diatoms, the transition metal zinc (Zn) is a component of nearly 300 enzymes involved in virtually all aspects of metabolism (Vallee and Auld 1990). In addition to its important role in alkaline phosphatase (Dyhrman and Ruttenberg 2006), zinc-finger transcription factors (Klug 2010), Cu/Zn superoxide dismutase (Alscher et al. 2002; Twining and Baines 2013), and photosystem II efficiency (Koch and Trimborn 2019), Zn^{2+} fulfills a catalytic role in carbonic anhydrase enzymes (CAs). It is well established that diatoms and most other aquatic photoautotrophs possess an inorganic carbon-concentrating mechanism (CCM) in which accumulated inorganic carbon is kept in the chloroplast as HCO_3^- and is rapidly interconverted with CO_2 in a process catalyzed by chloroplastic CAs in the vicinity of ribulose-1,5-biphosphate carboxylase/oxygenase (Rubisco). As the typical concentration of CO_2 in marine habitats (~16 μM) is lower than the half saturation constant (K_m) of Rubisco (20 - 70 μM in diatoms) (Young et al. 2016), the CCM allows photoautotrophs to maintain productivity at subsaturating ambient CO_2 concentrations (Colman and Rotatore 1995; Matsuda et al. 2001; Roberts et al. 2007). Both CAs and Zn^{2+} are thus key to photosynthetic CO_2 assimilation in marine phytoplankton,

3

particularly in rapidly growing and larger eukaryotic microbial photoautotrophs where the diffusive flux of CO_2 can limit growth rate (Riebesell et al. 1993).

To date, eight distinct subclasses of CA have been identified in nature and are designated by the Greek letters alpha, beta, gamma, delta, zeta, eta, theta and iota (α, β, γ, δ, ζ, η, θ, and ι) (DiMario et al. 2018), iota class being the most recently discovered (Jensen et al. 2019). While Zn^{2+} is the cofactor most commonly used in algal CAs, utilization of both cadmium (Cd^{2+}) and cobalt (Co^{2+}) in place of Zn^{2+} at the active site has been previously documented. For example, the diatom *Thalassiosira weissflogii*'s CA portfolio includes both a ζ-CA (CDCA) and a δ-CA (TWCA1) that are able to replace Zn^{2+} with Cd^{2+} and with Co^{2+}, respectively (Lee and Morel; Price and Morel 1990; Morel et al. 1994; Sunda and Huntsman 1995; Yee and Morel 1996; Lane et al. 2005).

The substitution of Cd^{2+} or Co^{2+} in place of Zn^{2+} in metalloenzymes such as CAs is hypothesized to confer a competitive advantage to substitution-capable phytoplankton species when faced with extremely low concentrations of bioavailable Zn. While there is currently limited evidence for primary oceanic Zn limitation (Coale 1991; Crawford et al. 2003), concentrations of surface total dissolved Zn (dZn) in low latitude ocean basins are scarce enough to warrant investigation into its potential. dZn concentrations in the central North Pacific are 0.15 - 0.35 nM in the surface mixed layer (Bruland 1989), a factor of 250 times lower than concentrations at depth (Lohan et al. 2002). The concentration of bioavailable Zn^{2+} is even lower, as ~98% of total dZn is complexed with Zn-binding organic ligands (Bruland 1989;

4

Ellwood and van den Berg 2000; Lohan et al. 2002; Bruland and Lohan 2003). This corresponds to a bioavailable Zn^{2+} concentration of 2 - 14 pM in the surface open Pacific (Donat and Bruland 1990). While metal organic complexes are known to be bioavailable under certain circumstances, transport across the cell membrane requires specialized transport systems whose rates tend to be quantitatively less important than inorganic acquisition pathways (Shaked et al. 2006; Aristilde et al. 2012), hence inorganic transport is likely still a major acquisition pathway. Based on limited culture studies and given the potential for oceanic Zn limitation, the use of Co (or Cd) in place of Zn in metalloenzymes likely allows marine phototrophs to at least partially compensate for metabolic Zn deficiency, providing an adaptive strategy to growth.

The Zn/Co substitution ability in marine phytoplankton has been investigated in previous studies by measuring specific culture growth rates as a function of Zn and Co added to the growth media, typically employing the metal buffer EDTA to control free-ion concentrations of Zn^{2+} and Co^{2+} (Price and Morel 1990; Sunda et al. 2005). Prior work regarding this substitution ability has only been investigated in a handful of representative model phytoplankton to date, but has suggested that a diverse array of $Zn^{2+}/Co^{2+}/Cd^{2+}$ substitution capabilities and efficiencies exist among phytoplankton. For example, Co has been shown to largely meet growth requirements during Zn limitation in the marine centric diatoms *Thalassiosira pseudonana*, *Thalassiosira oceanica,* and *Thalassiosira weissflogii* (Price and Morel 1990; Sunda and Huntsman 1995) and in the freshwater centric diatom *Cyclotella sp.* (Intwala et al. 2008). $Zn^{2+}/Co^{2+}/Cd^{2+}$ substitution has also been documented in the marine prymnesiophytes *Emiliania*

5

huxleyi and *Phaeocystis antarctica* (Sunda and Huntsman 1995; Timmermans et al. 2001; Xu et al. 2007; Saito and Goepfert 2008) and in the freshwater chlorophyte *Chlorella sp.* (Intwala et al. 2008). The presence of the Zn/Co substitution ability among eukaryotic phytoplankton is not universal, however, as *Chaetoceros calcitrans* has been shown to possess an absolute Zn requirement that cannot be met by Co (Timmermans et al. 2001). In contrast to the majority of marine phototrophic eukaryotes, the cyanobacteria *Synechococcus bacillaris* and *Prochlorococcus* MED4 both lack this ability and instead have an absolute Co requirement that cannot be met by Zn. This is hypothesized to be a vestigial trait carried over from their evolution in the ancient anoxic ocean, when Zn was scarce and Co more abundant (Sunda and Huntsman 1995; Saito et al. 2002, 2003).

In this study, we expand our understanding of the Zn/Co metabolic substitution capability in marine phytoplankton by conducting the first studies of this type on the marine pennate diatoms *Phaeodactylum tricornutum* and *Pseudo-nitzschia delicatissima*. We compare the growth responses of the Atlantic isolates *P. tricornutum* and *T. pseudonana* to those of the NE Pacific isolates *P. delicatissima* UNC1205 and *Thalassiosira sp.* UNC1203 (*Thalassiosira* UNC1203 herein) and relate these to the surface dissolved concentrations of Zn and Co in their native environments, including new metal data from the northeast Pacific Line P transect presented in this study. The relationship between the abundance of these trace metals in the field and the physiological response to Zn and Co limitation in diatoms is explored. For the purpose of dataset intercomparison, we have designed these growth rate studies after those conducted by

6

Sunda and Huntsman 1995, and similarly include the model diatom *Thalassiosira pseudonana* CCMP1335 in our investigation for replicability.

Materials and methods

Sample collection

Seawater samples were collected from the northeast Pacific aboard the RV Thomas G. Thompson (TN280) from 17-22 May 2012 (Fig. 1). Samples for trace element analysis were collected using the GEOTRACES sampling rosette system (Cutter and Bruland 2012). This system uses 12L Teflon coated GO-FLO sampling bottles (General Oceanics) mounted on a trace metal clean rosette that are preprogrammed to trip on the up cast at pre-specified depths. GO-FLO bottles were sampled inside a Class-100 clean van kept under positive pressure with HEPA-filtered air after the rosette was brought on deck. Total dissolved metal samples were collected into acid cleaned, sample rinsed, low-density polyethylene bottles (LDPE, Nalgene) after in-line filtration through 0.2 μm pore size Acropak capsules (Pall Corporation) using gas pressurization of the GO-FLO bottles with ultrapure N_2 gas. Samples were then acidified to pH ~ 1.4 by adding trace metal grade HCl (Fisher Optima). All critical ship board manipulations such as sample acidification and loading of the sampling filters were carried out inside a positive pressure ISO-sized 20 ft aluminum container built to US UNOLS standards (Cutter and Bruland 2012).

The LDPE sampling bottles were rigorously cleaned in a sequential four-step process before use. Bottles were soaked in a 5% Citranox acid detergent bath (Alconox) for at least a

7

day, soaked in a 10% hydrochloric acid bath (HCl; VWR) for at least a day, filled with 10% HCl and baked at 60°C upright and upside down (to properly leach the threads around the cap) for at least 2 days and filled with 0.1% trace metal grade HCl (Optima, Fisher) and baked at 60°C again for at least 2 days. In between each step, the insides and outsides of the bottles were thoroughly rinsed at least five times with Milli-Q water (18.2 MΩ; Millipore).

All samples were acidified to below pH 2 by the addition of concentrated trace metal grade HCl (Optima, Fisher) and stored for at least one month before analyses were made. 15 mL polypropylene centrifuge tubes (VWR) used for the sample preparation were cleaned in a two-step process. They were first soaked in 10% HCl at 60°C for 48 hours and rinsed at least five times with Milli-Q water. Following the soaks, the tubes were filled to a positive meniscus with 0.5% trace metal grade HCl and capped. They were then baked at 60°C overnight. Tubes were then filled with 0.5% trace metal grade HCl and were capped and stored until further use. Upon analysis, the tubes were emptied and rinsed seven times with Milli-Q water and at least once with sample before use.

Total dissolved Zn analysis

Total dissolved Zn concentrations were quantified using isotope dilution and magnesium hydroxide pre-concentration followed by analysis using inductively coupled plasma mass spectrometry (ICP-MS) as described previously (Wu and Boyle 1998; Saito and Schneider 2006; Jakuba et al. 2008). 13.5 mL of the acidified sample was poured into a pre-cleaned 15 mL centrifuge tube and then spiked with a ^{67}Zn spike (BDH Aristar Plus, VWR) and allowed to

8

equilibrate for a minimum of 1 hour. 125 μL of 11 mol L^{-1} ammonium hydroxide (Optima) was then added to each tube. After 90 sec, the tube was inverted and after an additional 90 sec, tubes were centrifuged for 3 min at 4000 rpm using a swinging bucket centrifuge (Eppendorf). The resulting supernatant was decanted carefully before tubes were respun for 3 min to form a firm pellet and the remaining supernatant was shaken out. Pellets were stored dry until the day of analysis (no longer than a few days). Pellets were dissolved on the day of ICP-MS analysis using 1.5 mL of 5% nitric acid (Optima). ICP-MS measurements were made using a Finnigan ELEMENT2 in medium resolution mode, which was sufficient to resolve ^{64}Zn from the potential interference peak due to the MgAr$^+$ ion. The reported values have had the procedural blank subtracted. To measure the procedural blank, 1 mL of low Zn surface seawater was treated as the samples but calculations were performed as though it was a 13.5 mL sample (Zn contribution from the 1 mL is considered negligible). The average blank value was 0.14 nmol L^{-1} and the average detection limit was 0.08 nmol L^{-1}. Procedural seawater blanks were prepared the same way as samples using 1 mL low trace metal surface seawater from the 2004 SAFe cruise. The average blank value was 0.08 nmol L^{-1} and the average detection limit (measured as thrice the standard deviation of the blank) was 0.06 nmol L^{-1}. The accuracy of the method was evaluated by measuring GEOTRACES reference standards GS and GD (Johnson et al. 2007). The Zn values obtained by this method for GS and GD were 0.04 ± 0.007 nmol L^{-1} and 1.67 ± 0.002 nmol L^{-1}, respectively, and were in agreement with certified consensus Zn values of 0.038 ± 0.011 nmol L^{-1} (GS) and 1.64 ± 0.22 nmol L^{-1} (GD).

Total dissolved Co analysis

Sample and reagent bottles were cleaned to remove trace metal contaminants before use. Bottles were soaked for at least one week in the acidic detergent Citranox, rinsed thoroughly with 18.2 M-Ohm Milli-Q water (Millipore), filled with 10% HCl to soak for 10 days, and rinsed thoroughly with Milli-Q water adjusted to pH 2 with TM-grade HCl. Reagent purification protocols were identical to those previously published (Saito and Moffett 2001). Total dissolved cobalt concentrations were determined using cathodic stripping voltammetry (CSV) as described previously (Saito and Moffett 2001; Saito et al. 2004). Dissolved cobalt measurements were made using an Eco-Chemie µAutolabIII system with a Metrohm 663 hanging mercury drop electrode and Teflon sampling cups, in addition to a Metrohm 837 autosampler system operated with NOVA 1.8 software (Metrohm Autolab B.V.).

Seawater samples were UV-irradiated for 1 h prior to analysis using a Metrohm 705 UV digester to degrade organic cobalt-binding ligands, enabling full chelation by the added electroactive ligand, dimethylglyoxime (DMG). 11 mL of sample was pipetted into 15mL polypropylene tubes. Recrystallized DMG (0.1M in methanol) was added to a final concentration of 400 µM, and purified N-(2-hydroxyethyl)piperazine-N-(3-propanesulfonic acid) (EPPS) buffer (0.5 M in Milli-Q water) was added to a final concentration of 3.8 mM. Tubes were inverted several times before being placed in the autosampler queue. 8.5 ml of the mixture was dosed into the Teflon analysis cup using a 800 Dosino automated burrette (Metrohm). 1.5 mL of

10

purified sodium nitrite (1.5M in Milli-Q water) was added directly to the Teflon cup using a dedicated 800 Dosino burrette. Samples were purged with high purity (>99.99%) N_2 for 3 min once loaded. Cobalt concentrations were determined by standard addition, with triplicate measurement of the sample followed by four 25 pM cobalt additions. 5 nM Co stock was diluted from a certified 1ppm reference (SPEX) and added to the analysis cup via a third Dosino burrette.

The analytical blank was determined by analyzing seawater that had been UV-irradiated for 1 h, equilibrated overnight with prepared Chelex 100 resin beads (Bio-Rad), and UV-irradiated a second time to degrade any leached synthetic ligands. The mean blank was 4.6 +/- 0.7 pM, and the detection limit was calculated as triple the standard deviation of the blank (2.1 pM). The Saito laboratory has participated in the GEOTRACES intercalibration effort using this electrochemical Co method. Acidified standards were neutralized with concentrated ammonium hydroxide (Seastar), mixing the entire sample between drops, prior to UV digestion. Using this electrochemical method, our laboratory values for the GEOTRACES and SAFe standard analyses (including those conducted during analysis of the EPZT samples, which were analyzed within the same year) were: SAFe D1 = 48.5 ± 2.4 (n=3, at sea), SAFe D2 = 45.0 ± 2.7 (n=7), GEOTRACES GSP = 2.5 ± 2.0 (n=10), GEOTRACES GSC = 77.7 ± 2.4 (n=4). These Co values agree well with those of the GEOTRACES intercalibration effort, demonstrating that the electrochemical methodologies used to produce the dCo dataset presented in this study detect Co concentrations within the standard deviation of current consensus values

for UV irradiated samples. Current consensus values can be found on the International

GEOTRACES Program Website (http://www.geotraces.org/).

Media and diatom culturing techniques

   Thalassiosira pseudonana CCMP1335 cultures were maintained in a 24°C incubator

under constant fluorescent lighting (65 μmol quanta m^{-2} s^{-1} PAR). *Phaeodactylum tricornutum*

CCMP632 cultures were maintained in an 18°C incubator under constant fluorescent lighting (90

μmol quanta m^{-2} s^{-1} PAR). Both Northeast Pacific *Pseudo-nitzschia delicatissima* UNC1205 and

Northeast Pacific *Thalassiosira sp.* UNC1203 were grown in an 18°C incubator under constant

fluorescent lighting (85 μmol quanta m^{-2} s^{-1} PAR). All cultures were randomly repositioned each

day to avoid any effect of subtle variation in light intensity on growth. *T. pseudonana*

CCMP1335 and *P. tricornutum* CCMP632 (Bigelow Laboratory, East Boothbay, ME) were

obtained from the Mincer and Saito laboratory culture collections at the Woods Hole

Oceanographic Institution, respectively. NE Pacific *P. delicatissima* UNC1205 and *Thalassiosira*

sp. UNC1203 were obtained from the Marchetti laboratory at the University of North Carolina.

Both NE Pacific isolates were collected at station P8 of Line P, a northeast Pacific ocean transect

located off of Vancouver Island comprising 26 sampling stations and ending at Ocean Station

Papa at 50°N 145°W (Fig. 1a). All cultures were axenic and maintained by sterile technique until

needed.

   Polycarbonate and plastic bottles were cleaned to remove trace metal contaminants

before use. This procedure involved, at minimum, a 72h soak in <1% Citranox detergent, five

rinses in Mili-Q water, a 7 day soak in 10% HCl, and five rinses with dilute acid (HCl, pH 2). Cultures were grown in microwave sterilized 28 mL polycarbonate centrifuge tubes, and all solutions were pipetted only after a tip rinse procedure consisting of three rinses with 10% HCl followed by three rinses with sterile dilute HCl (pH 2). All culture work was conducted in a Class 100 clean room.

Culture media was prepared after that used by Sunda and Huntsman for trace metal experimentation (Sunda and Huntsman 1995). Microwave sterilized, 0.2 μm-filtered Pacific seawater from the North Pacific station "Aloha" (22° 45'N, 158° 00'W) was used as the media base. Macronutrients were added to this sterile base to a final concentration of 88.2μM $NaNO_3$, 41.5μM NaH_2PO_4, and 106μM Na_2SiO_3 and were chelexed before use. Added vitamins included 2 nM biotin, 0.37 nM B_{12} as cyanocobalamin, and 300 nM thiamine and were also chelexed before use. Trace metals were added to final media concentrations of 10^{-7} M $FeCl_3$, 4.8 x 10^{-8} M $MnCl_2$, 4.0 x 10^{-8} M $CuSO_4$, 10^{-7} M $NiCl_2$, and 10^{-8} M Na_2O_3Se within a 10^{-4} M ethylenediamine tetraacetic acid disodium salt (EDTA, Acros Organics, $C_{10}H_{14}N_2Na_2O_8$) metal ion buffer system. All media amendments were sterile filtered through acid rinsed 0.2μm filters before addition to final media, and final media equilibrated for at least 12h before inoculation.

Established cultures of each diatom were first acclimated in low-metal media containing 1 nM total Zn or less for at least three transfers. These acclimated cultures were used to inoculate initial cultures at 1% volume. For all diatoms, Zn or Co limitation experiments were first performed using a range of added Zn concentrations with Co omitted and vice versa. We refer to

13

growth rate experiments using media amended with Zn *or* Co (while omitting the other) as "simple limitation" experiments. Growth rate experiments varying concentrations of both Zn and Co (which we refer to as "matrix" experiments) were also conducted, allowing for three-dimensional visualizations of growth rates as used previously (Saito et al. 2002; Saito and Goepfert 2008). Growth of all experiment cultures was monitored by relative chlorophyll fluorescence using a Turner TD-700 fluorometer, calibrated prior to measurement with a solid standard. Growth rates were calculated as the slope of the natural logarithm of the increase in chlorophyll fluorescence over a four-measurement (usually 4 day) period during exponential growth. Computed ratios of $[Zn^{2+}]$ and $[Co^{2+}]$ to total concentrations, whose values are $10^{-3.99}$ and $10^{-3.63}$ respectively, were used to convert total added metal concentrations to free ion concentrations and are the same as those used by Sunda and Huntsman (Sunda and Huntsman 1995). Half-saturation constants (K_m) for growth and maximal growth rates (μ_{Max}) were calculated from simple limitation growth rates using a nonlinear fitting function in MATLAB (MathWorks Inc.). Ocean sections were created in Ocean Data View (Schlitzer 2011).

Metal quotas

Cellular metal quotas were measured by inductively coupled plasma mass spectrometry (ICP-MS). Biomass from replicate 25 mL matrix cultures of *P. tricornutum* CCMP632, *P. delicatissima* UNC1205, and *Thalassiosira* UNC1203 were pooled upon entering stationary phase and were centrifuged at 11,000 RPM (14,610 x g) for 40 minutes at 4°C. The cell pellet was resuspended in ~1 mL media and transferred to an acid-cleaned microcentrifuge tube.

14

Cultures were centrifuged again for 30 min at 14,100 RPM (13,336 x g) at 4°C before the supernatant was discarded. The remaining cell pellet was acidified in 800 μL of 5% nitric acid (Optima) containing 1 ppb indium for at least seven days. Solids were removed by centrifugation. No attempt was made to remove extracellular metals by washing cells with additional metal chelators in order to minimize processing blanks. Quota determinations therefore include contributions from both intracellular and extracellular pools. Process blank digestions containing acid but no cells were performed in parallel. Digests were diluted by a factor of 9 with 5% nitric acid 1 ppb indium solution before being analyzed in duplicate on a Thermo ICAP-Q plasma mass spectrometer calibrated to a multi-element standard curve (Spex Certiprep) over a range of $1 - 20$ ppb. Samples were analyzed in KED mode after an 85s sample uptake window and element mass windows were scanned 3 times during measurements. The 1 ppb indium internal standard was used to correct for variation in sample delivery and plasma suppression between samples. Process blanks were subtracted from measured concentrations. Phosphorus concentrations were also measured by ICP-MS simultaneously and were calibrated to a standard curve ranging from $100 - 3,200$ ppb using a 1 ppm certified P stock (Alfa Aesar Specpure). The seawater media base used for all growth experiments was similarly analyzed via ICP-MS using a 1:10 dilution of media base into 5% nitric acid 1 ppb indium and analyzed as above to determine background media concentrations of total Zn and Co (0.9 nmol L^{-1} and 0.1 nmol L^{-1}, respectively).

Cell-specific field metal quotas

Metal contents of individual diatom cells were measured with synchrotron X-ray fluorescence (SXRF; Twining et al. 2003) following protocols described previously (Twining et al. 2015). Briefly, unfiltered seawater from 30m and 60m GO-Flo bottles was fixed with glutaraldehyde (0.25% final concentration of cleaned, EM-grade glutaraldehyde) and centrifuged onto C/formvar-coated Au TEM grids (200 mesh, Electron Microscopy Sciences). The supernatant was gently discarded and grids removed from the centrifuge tubes. Grids were rinsed with a drop of deionized water ($>18\ \text{M}\Omega$), water immediately wicked away, and then stored in a vacuum-sealed, dark chamber until analysis.

Cellular metals were analyzed with the 2-ID-E Microprobe beamline at the Advanced Photon Source, Argonne National Laboratory. Incident beam energy was 10 keV to enable the excitation of K_α fluorescence for elements ranging in atomic number from Si (14) to Zn (30). Approximately 10-15 individual cells were analyzed at each station and depth. Element quantification was performed by averaging the spectra from pixels representing the cells of interest. Spectra were also extracted from a background area close to each cell. The spectra from each of four elements of Vortex ME4 detector were then separately fit and averaged with MAPS, a custom fitting software package (Vogt 2003). Concentrations were calculated based on conversion factors obtained by running the thin-film standards NBS 1832, NBS 1833, AXO C_0 (AXO Dresden GmbH, Germany). Cell volume was calculated based on measurements taken from bright field images of the cells and using the equations of Hillebrand et al. 1999 (Hillebrand

et al. 1999). Cellular C was then calculated from the volumes using the equations described in Menden-Deuer and Lessard 2000 (Menden-Deuer and Lessard 2000).

Particulate trace metals

Particulate Co and Zn were analyzed following protocols described in Twining et al. 2015. GO-Flo bottles were over-pressurized to approximately 34.5 kPa with 0.2 µm filtered air and seawater passed through 25 mm 0.4 µm Pall Supor filter membranes. Filtration continued until the GO-Flo bottle was empty or 2 h had elapsed. Filtrate was collected and measured to determine the filtered volume. Excess water was removed from the filter membrane by applying gentle vacuum after which the membrane was transferred to an acid washed petri-slide, double bagged, and kept frozen at -20°C for analysis on shore.

Labile and total particulate concentrations were analyzed through sequential digestion of the Supor membranes following the protocol of Rauschenberg & Twining 2015 (Rauschenberg and Twining 2015). Membranes were first leached using an acetic acid-hydroxylamine solution to solubilize labile elements (Berger et al. 2008). The membranes were then transferred to a PFA vial and digested with a 4M HCl/4M HNO$_3$/4M HF mixture to solubilize any remaining particulate material (Ohnemus et al. 2014). Cesium was spiked into the acetic acid solution as a means of monitoring recovery and carryover from the first leach into the second digest. The reference materials and process blanks – filters that had 2 L of 0.2 µm filtered seawater passed through them – were sequentially digested alongside the samples. Digests were analyzed using a Thermo Element2 HR-ICP-MS equipped with a quartz nebulizer, cyclonic spray chamber, and

17

nickel cones. In-115 was used as a drift monitor, and quantification was performed using external calibration curves.

Data repository

The environmental trace metal data, diatom growth rate data, and diatom metal quota data presented in this paper have been deposited into the Biological and Chemical Oceanography Data Management Office (BCO-DMO) database (http://bcodmo.org/).

Results

dZn and dCo concentrations of diatoms' native environments

Before conducting Zn and Co growth rate experiments on four marine diatom species, we first examined the total dissolved concentrations of Zn (dZn) and Co (dCo) measured in each species' native environment. For the Atlantic isolates *T. pseudonana* and *P. tricornutum*, we relied on previously reported surface dZn and dCo values found in the literature. In the Atlantic and other ocean basins, dCo is usually less abundant than dZn with typical surface dCo:dZn ratios ranging from 0.05:1 M – 0.11:1 M (Ellwood and van den Berg 2000; Nolting et al. 2000; Bowie et al. 2002; Jakuba et al. 2008; Noble et al. 2017) (Table 1).

For our Northeast (NE) Pacific isolates *P. delicatissima* and *Thalassiosira* UNC1203, we report new dissolved metal data from the NE Pacific Line P transect. dZn was strongly depleted throughout the transect, with surface concentrations reaching as low as 0.03 nM (Fig. 1b, Fig. 2a). Depth profiles of dZn at each station were nutrient-like, with characteristic removal of dZn into the particulate phase at the surface with regeneration at depth (Fig. 2a), similar to previously

18

described north Pacific dZn profiles (Bruland et al. 1978; Lohan et al. 2002; Jakuba et al. 2012; Vance et al. 2019). Surface dZn concentrations < 0.1 nmol kg^{-1} have also been reported previously at the coastal station P4 (Vance et al. 2019).

For dCo, the combined effects of nutrient uptake and scavenging resulted in hybrid-type depth profiles at stations P5, P6 and P8 with evidence of surface minima due to biological uptake, subsurface maxima due to regeneration, and deeper depletion due to scavenging (Fig. 2a). Scavenging of dCo is an important mechanism for dCo removal and involves the co-precipitation of dCo into Mn oxides by Mn-oxidizing bacteria as Co is oxidized from Co(II) to Co(III) (Cowen and Bruland 1985; Moffett and Ho 1996; Swanner et al. 2014). Hybrid-type profiles for dCo in the Pacific have been observed previously (Knauer et al. 1982; Noble et al. 2012; Ahlgren et al. 2014; Saito et al. 2014). Closer to shore, dCo did not exhibit these hybrid-type profiles but rather exhibited surface maxima at stations P1 and P4 that decreased with depth, and more nutrient-like behavior at stations P2 and P3 (Fig. 2a). The variability among the dCo profiles is not unusual given the complexity of Co cycling, which is influenced by biological uptake, remineralization, scavenging, and abiotic inputs (Saito et al. 2017). Across all stations, however, measured surface concentrations were particularly high for dCo, reaching ~200 pM (Fig. 1c, Fig. 2a). The surface concentrations of dCo measured in this study are therefore 4x larger than Pacific surface dCo concentrations of ~10 – 50 pM measured previously in the North Pacific subtropical gyre and Gulf of Alaska (Martin et al. 1989; Noble et al. 2008). Although dCo plumes >100 pM have been observed previously, these high concentrations were present in

19

oxygen minimum zones (OMZs: dissolved $O_2 < 100\mu M$) with associated upwelling systems. For example, OMZ-supported dCo plumes exceeding 100 pM have been found in the Benguela and Mauritanian upwelling systems in the Atlantic (Noble et al. 2012, 2017) and in the Costa Rica dome, California margin, and central and south Pacific (Biller and Bruland 2013; Ahlgren et al. 2014; Saito et al. 2014; Hawco et al. 2016). Reductive dissolution of sedimentary Mn oxides under low O_2 conditions is thought to release a large flux of dCo that is then advected and upwelled (Sundby et al. 1986; Saito et al. 2004; Hawco et al. 2018).

Dust deposition does not appear to be the source of the observed surface dCo values, as the mean dry and wet dust deposition over Line P and in the general Gulf of Alaska area was negligible during 2012 ($< 0.1 \times 10^{-11}$ kg m^{-2} s^{-1}) (Sim and Orians 2019), and dCo supply to the oceans via dust is known to be minimal overall (Tagliabue et al. 2018). We find a weak correlation between dCo and salinity in this transect ($R^2 = 0.34$; Fig. 3a), implying a potential freshwater source. Further work investigating the contributions of dissolved and particulate Co from the major watersheds affecting Line P is needed. In contrast to dust and fluvial sources, sediments are the major external driver of both surface and interior dCo distributions. Enhanced sedimentary Co fluxes at low dissolved O_2 levels have been modelled to reproduce Co distributions in the tropics, whereas sedimentary Co fluxes can be reproduced by large shelf areas in the Arctic (Tagliabue et al. 2018). We observed an OMZ ($dO_2 < 100\mu M$) between 200 and 2000 m, with the lowest dissolved O_2 found at ~900 m (7.9 μmol kg^{-1}) across the transect (Fig. 1e). While we did not find evidence of a correlation between dCo and dissolved O_2 in this

20

coastal dataset (Fig. 3b) likely due to proximity to riverine inputs and complex circulation, a recent study has shown that the northeast Pacific is experiencing a significant decline in dissolved O_2 with a net loss of $11.7 \pm 3.5\%$ (high compared to the global average of 2%) in total oxygen content per square meter over six decades (Cummins and Ross 2020), implying that dCo in this region has the potential to further increase with deoxygenation. The observed distribution of dCo was also not coincident with that of dMn, implying that the reduction of Mn oxides was not the major dCo source (Fig. 1c,d). High (> 70 pM) surface dCo concentrations have previously been reported for the NE Pacific subpolar gyre area and were ascribed to continental shelf sources (Zheng et al. 2019). We therefore hypothesize that the high surface dCo values observed at Line P most likely resulted from a combination of shelf input and fluvial sources.

The abundance of dCo and depletion of dZn at the surface gave rise to dCo:dZn ratios along Line P that exceeded 1, ranging from 0.03:1 to 3.52:1 at surface (1 – 100 m) depths (Fig. 2b). These surface ratios are the highest we are aware of to date, as illustrated by comparison of these ratios at Line P to those of the North Atlantic (NAZT) and Eastern Pacific (EPZT) (Fig. 4). In contrast to the dissolved ratios, the total particulate ratio of pCo:pZn was consistently less than 1:1. pZn was consistently ~25x larger than pCo throughout the transect at the surface (Fig. 2c), implying a high biological Zn demand. The severe depletion of dZn at the surface corroborates this, and the resulting abundance of dCo in relation to dZn likely created selection pressure for phototrophs that were able to use Co once Zn was depleted in this ecosystem. The metal quotas of single diatom cells sampled from the Line P transect also demonstrated the high biological

21

demand for Zn. Zn quotas were consistently higher than Co quotas for diatoms across four stations of Line P, though these showed a marked decrease moving offshore from station P1 to P4 (Fig. 10a). Interestingly, the Co quotas of these diatom cells tended to increase moving offshore (Fig. 10b), though these Co quotas were ~150 – 1000x smaller than Zn quotas measured in the same cells such that cellular Co:Zn ratios were ~0.01 mol:mol (Fig. 10c).

Diatom growth rate and metal quota experiments

We next assayed Zn/Co metabolic substitution in four different diatom species by measuring the effect of free ion concentrations of Zn^{2+} and Co^{2+} on specific growth rate. We explored the growth response of each diatom species in Zn vs. Co-amended media to assess their metabolic capacity to substitute these metals. Notably, the media composition was consistent across these experiments, allowing results to be intercomparable among species. Furthermore, we measured the total intracellular and extracellular metal content following the completion of the growth rate studies to investigate differences in total metal content.

Atlantic T. pseudonana CCMP1335

We designed our growth rate experiments after those used by Sunda and Huntsman 1995 and included the Atlantic diatom *T. pseudonana* CCMP1335 as used in their study to gauge replicability. Increasing Zn^{2+} concentrations caused increased growth rates in *T. pseudonana* to a maximum of 0.72 d^{-1}. Increasing Co concentrations also caused increased growth rates in this diatom, but only to a maximum of 0.38 d^{-1}. Growth rates achieved with Zn additions were consistently higher than growth rates achieved with Co additions (Fig. 5a, Table 2) suggesting a

"preference" for Zn, in agreement with the findings of Sunda and Huntsman 1995. This Zn preference was also evident in the higher biomass yields achieved with Zn additions compared to Co additions (RFU, Table 2). The fact that Co additions were able to partially restore the growth rate of *T. pseudonana* in media lacking Zn demonstrates a Zn/Co substitution capability in this diatom (Fig. 5a, Fig. 7a), also consistent with Sunda and Huntsman 1995. Matrix experiments, in which both Zn and Co were added to the growth media and covaried, resulted in a plateau of consistent growth rates that averaged ~0.65 d^{-1} (Fig. 7a, Table 2).

Atlantic P. tricornutum CCMP632

Like *T. pseudonana*, the growth rate of Atlantic *P. tricornutum* increased in response to increasing concentrations of added Zn or Co in simple limitation experiments (Fig. 5b, Fig. 7b). Also like *T. pseudonana,* growth rates in all simple Zn additions exceeded those in comparable Co additions (Fig. 5b). However, unlike *T. pseudonana*, this diatom was still able to grow in unamended "blank" media ($\mu = 0.60$ d^{-1}). Maximum growth rates were 0.80 d^{-1} in simple Zn addition and 0.78 d^{-1} in simple Co addition (Fig. 5b, Table 3), thus $\mu_{MaxCo} \approx \mu_{MaxZn}$ for this diatom (Fig. 6). Interestingly, the same growth rate of 0.80 d^{-1} was observed in response to increasing [Zn^{2+}]. This diatom's growth rate therefore appeared to plateau at 0.80 d^{-1} in [Zn^{2+}] $\geq$ 1.1 x 10^{-12} M (Fig. 5b). Like *T. pseudonana,* a metabolic Zn/Co substitution ability in *P. tricornutum* was evident given its ability to increase growth rates in Zn-amended media omitting Co and in Co-amended media omitting Zn (Fig. 5b, Fig. 7b).

Thalassiosira UNC1203

The growth response of NE Pacific *Thalassiosira* UNC1203 to Zn and Co additions was strikingly different compared to Atlantic *T. pseudonana*. Growth rates of *Thalassiosira* UNC1203 in all Co treatments were higher than the growth rates achieved in comparable Zn treatments (Fig.5c, Table 4), opposite of that observed in *T. pseudonana*. Over this range of added metal amendments, NE Pacific *Thalassiosira* thus demonstrated a Co preference rather than a Zn preference. In contrast to both Atlantic diatoms, the maximum growth rate of *Thalassiosira* UNC1202 achieved with Co addition ($\mu_{\text{MaxCo}} = 0.35$ d^{-1}) was significantly higher than the maximum growth rate achieved with Zn addition ($\mu_{\text{MaxZn}} = 0.30$ d^{-1}) (Fig. 6) as determined by an unpaired (2 sample) t test assuming equal variances. Notably, the Co preference of this diatom was also reflected in the higher biomass yields in all simple Co amendments compared to all simple Zn amendments (RFU, Table 4). In matrix experiments, as observed in the other diatoms, addition of both Zn and Co resulted in growth rates that were higher than those achieved by addition of one metal alone, to a maximum of 0.39 d^{-1} (Fig. 7c, Table 4). Overall, this diatom demonstrated a Zn/Co substitution capability and an apparent Co preference.

P. delicatissima UNC1205

The other NE Pacific isolate, *P. delicatissima* UNC1203, also demonstrated Zn/Co metabolic substitution with growth in both Zn-amended media lacking Co and vice versa (Fig. 5d). Like *Thalassiosira* UNC1203, the maximum average growth rate of *P. delicatissima* achieved with Co additions ($\mu_{MaxCo} = 0.75$ d^{-1}) exceeded the maximum average growth rate

achieved with Zn additions ($\mu_{MaxZn} = 0.70$ d^{-1}) (Fig. 6), though these were not significantly different as determined by an unpaired t test assuming equal variances. Unlike *Thalassiosira* UNC1203, *P. delicatissima* did not demonstrate a clear Co preference. In fact, a Zn preference was not evident either. Instead, growth rates in all Zn additions were closely comparable to growth rates in all Co additions (Fig. 5d), implying a highly efficient Zn/Co substitution ability that allowed this diatom to maintain high growth rates when provided with either metal. Unlike *T. pseudonana*, *P. tricornutum,* and *Thalassiosira* UNC1203, additions of both Zn and Co in matrix additions produced what appeared to be a highly efficient metabolic substitution capability in regards to growth rate. This is evident in the consistently high matrix growth rates (0.83 d^{-1} to 0.97 d^{-1}) that occurred over all matrix treatments (Fig. 7d; Table 5). These treatments corresponded with higher biomass yields compared to those achieved with addition of Zn or Co alone (Table 5).

Culture cellular metal quotas

Upon reaching late log phase, biomass from selected matrix cultures of Atlantic *P. tricornutum,* NE Pacific *Thalassiosira* UNC1203, and NE Pacific *P. delicatissima* was harvested and analyzed for cellular Co, Zn, and Cd metal content. Notably, in the NE Pacific isolates *Thalassiosira* UNC1203 and *P. delicatissima,* their Zn:P quotas were on the same order of magnitude as their Co:P quotas in all measured culture treatments (0.01 – 1 mmol metal mol^{-1} P; Fig. 8c,d). In contrast, the Atlantic diatom *P. tricornutum* exhibited Zn:P quotas (0.01 – 2.36 mmol Zn mol^{-1} P) that were much larger than its Co:P quotas (0.0003 – 0.02 mmol Co mol^{-1} P)

(Fig. 8a,b). Furthermore, Zn and Co metal quotas of the NE Pacific diatoms revealed a "switchover" between cellular Zn and Co content as a function of added metal concentration. As Zn concentration increased, Zn quotas also increased while Co quotas fell (Fig. 8c,d; Fig. 9c,e). This trend was not apparent in the Atlantic *P. tricornutum,* which instead exhibited a peak in maximum cellular Zn (2.36 mmol Zn mol^{-1} P) corresponding with the highest amount of added Zn and Co (Fig. 8a; Fig. 9a; Table 7).

Discussion

In this study, we present physiological evidence demonstrating the ability of the diatoms *T. pseudonana* CCMP1335, *P. tricornutum* CCMP632, *Thalassiosira* UNC1203 and *P. delicatissima* UNC1205 to metabolically substitute Zn and Co as assessed by growth rate. Each of these diatoms grew in media amended with Zn but lacking additional Co and vice versa, demonstrating metabolic substitution of these trace metals (Fig. 5; Fig. 7). In the Atlantic diatoms *T. pseudonana* and *P. tricornutum,* Zn additions resulted in higher growth rates compared to Co additions (Fig. 5a,b; Fig. 6). Both Atlantic diatoms thus demonstrated a Zn preference over this range of added metal amendments. Co additions also stimulated growth, but growth rates were not as high as those achieved with Zn additions alone. For example, Co additions yielded a maximum growth rate in *T. pseudonana* that was only about 50% of that achieved with Zn additions (Table 2; Table 6), similar to the findings of Sunda and Huntsman 1995 in which the maximum growth rate of the same strain of *T. pseudonana* in Co was only 60% of that in Zn. Maximum growth rates found in this study likely differ from those found by

26

Sunda and Huntsman due to differences in incubation methods and light intensities (14/10 L/D cycle of 500 μmol quanta m^{-2} s^{-1} PAR compared to a constant 65 μmol quanta m^{-2} s^{-1} PAR used in this study).

Analysis of total cellular Zn and Co content highlighted the differences in Zn/Co use between Atlantic and NE Pacific diatoms and among the NE Pacific diatoms themselves. While both NE Pacific diatoms *P. delicatissima* and *Thalassiosira* UNC1203 achieved similar maximum Co quotas (0.44 and 0.40 mmol Co mol^{-1} P, respectively) (Fig. 8c,d; Fig. 9c,e; Table 7), the magnitude of their Zn quotas was quite different. Compared to *P. delicatissima*, in which Zn:P quotas ranged from ~0.2 – 0.8 mmol Zn mol^{-1} P, *Thalassiosira* UNC1203 appeared to maintain lower Zn quotas overall even in Zn replete conditions (Fig. 8c; Fig. 9c; Table 7), implying a lower overall baseline Zn requirement for this diatom. Cellular Zn and Co quotas were similarly investigated in *P. tricornutum*, a diatom isolated from the Atlantic where surface dCo:dZn ratios range from 0.05:1 – 0.11:1 (Table 1). While cellular Zn:P and Co:P quotas in the NE Pacific diatoms *P. delicatissima* and *Thalassiosira* UNC1203 were on the same order of magnitude, *P. tricornutum* exhibited Zn:P quotas that were about two orders of magnitude larger than its Co:P quotas (Fig. 8a,b). We thus found higher Zn quotas in the Atlantic diatom, which was isolated from an environment where surface dZn abundance exceeds dCo (Table 1). The Co:P quotas observed in Atlantic *P. tricornutum* agree well with previously reported P-normalized quotas for diatoms collected from the Equatorial Pacific, which averaged about ~0.1 mmol Co mol P^{-1} (Twining et al. 2011; Twining and Baines 2013). Zn:P quotas were lower than

27

those of average temperate Pacific diatoms (5 mmol Zn mol P^{-1}; Twining and Baines 2013) in all three diatoms, but were highest in Atlantic *P. tricornutum* (Table 7). Cd:P ratios in all three diatoms were also comparable, ranging from 0.02 to 0.22 μmol Cd mol P^{-1}, and decreased in response to increasing $[Zn^{2+}]$ (Fig. 9; Table 7).

The steady-state uptake rates of Zn, Co and Cd were also calculated for selected matrix treatments of Atlantic *P. tricornutum* and the NE Pacific diatoms *Thalassiosira* UNC1203 and *P. delicatissima*. Under steady state conditions, the net uptake rate (ρ) is equal to the cellular metal quota (Q) multiplied by the specific growth rate (μ) (Sunda and Huntsman 1995). The uptake rates of all three metals exhibited trends similar to those of the metal:P quotas in *P. tricornutum* and in *P. delicatissima* (Fig. 9b,f). In both of these diatoms, the uptake rate of Zn (ρZn) increased with increasing $[Zn^{2+}]$ while ρCo decreased (Fig. 9; Table 7). In contrast, the uptake rates of these metals in NE Pacific *Thalassiosira* UNC1203 were fairly constant over this range of added $[Zn^{2+}]$ (Fig. 9d). This further highlights the differences in Zn/Co metabolic use between the Co preferring *Thalassiosira* UNC1203 and the apparent lack of a metal preference in *P. delicatissima*.

Although the specific biochemical pathways conferring these differences are not yet understood, we can consider at least two ways in which cellular Zn/Co interactions may differ among species. At the cell surface, species may possess Zn and Co transport systems that operate at different efficiencies, or may possess shared transport systems that give rise to competitive inhibition effects. At the protein level, use of Zn versus Co as a cofactor may result in different

levels of enzyme activity. We have shown that *P. delicatissima* was able to grow equally well using either metal (Fig. 5d) and exhibited Zn and Co quotas of similar magnitudes (Fig. 9e). We thus posit that this diatom may possess both efficient transport systems and efficient substitution of Zn and Co at the enzyme level. As *Thalassiosira* UNC1203 demonstrated higher specific growth rates in Co alone (Fig. 5c), Co quotas that were larger than its Zn quotas (Fig. 9c), and Co uptake rates larger than Zn uptakes rates (Fig. 9d), we posit that this diatom may possess a highly efficient Co transport system. Further proteomic work is needed to investigate these potential transporters.

It is well established that Mn, itself an essential micronutrient, can compete with Cd, Co and Zn for transport sites at the cell surface and consequentially give rise to competitive inhibition effects in marine phytoplankton (Sunda and Huntsman 1996, 2000; Hawco and Saito 2018). For example, *T. pseudonana* possesses a membrane transport system with a shared affinity for Mn, Zn, and Cd with different affinity constants ($10^{7.1}\,M^{-1}$, $10^{7.5}\,M^{-1}$, and $10^{8.1}\,M^{-1}$, respectively; Sunda and Huntsman 2000). As described by the Irving–Williams series (Mn<Fe <Co<Ni<Cu>Zn), the smaller atomic radii and greater crystal field stabilization energy for Cu, Zn, and Ni causes these metals to form stronger organic complexes with organic ligands and to effectively compete against other divalent cations, such as Mn, for similar binding sites (Irving and Williams 1953; Waldron et al. 2009). The Mn uptake system therefore binds Zn and Cd more strongly than it does Mn. As Mn^{2+} interacts weakly with EDTA and natural organic ligands, inorganic Mn (Mn') is the most abundant transition metal ion in seawater and in the f/2

29

media used in this study (Sunda et al. 2005). Based on the measured total background concentration of Mn in our base seawater media (8.36 nM), the total amount of added $MnCl_2$ in the trace metal mix (48 nM), and the computed ratio of free Mn ions to total Mn concentration based on equilibration with 10^{-4} M EDTA ($10^{-1.23}$; Sunda and Huntsman 1996), we estimate the free Mn' concentration in our growth media to be 3.32 nM. Even at the highest added concentrations of Zn and Co used in this study, this Mn' concentration is still roughly 300 times more abundant than Zn^{2+} and 100 times more abundant than Co^{2+}. High Mn quotas were expected for all diatoms as an artifact of the high Mn' present in the culture media, but we still find a distinction between the NE Pacific and Atlantic diatoms. Mn quotas in the NE Pacific diatoms ranged from $2 – 4.5$ mmol Mn mol P^{-1}, similar to the range of Mn quotas previously observed in *Thalassiosira pseudonana* grown in the same Mn^{2+} media concentration as used in this study ($1.5 – 3$ mmol Mn mol P^{-1}, media $\log[Mn^{2+}] = -8.5$) (Sunda and Huntsman 1998). *P. tricornutum* had comparatively lower Mn quotas ($0.1 – 1.5$ mmol Mn mol P^{-1}) given the same media amendments (Fig. 11a). Furthermore, while decreasing Mn uptake rates at elevated $[Zn^{2+}]$ due to competitive inhibition effects were observed in both NE Pacific diatoms, this effect was not observed in Atlantic *P. tricornutum,* which maintained low (< 0.1 mmol Mn mol $P^{-1} d^{-1}$) uptake over all concentrations of $[Zn^{2+}]$ (Fig. 11b). *P. tricornutum* thus exhibited lower Mn quotas and uptake rates compared to the other diatoms, implying a uniquely low Mn requirement under these Zn/Co conditions that warrants further study.

30

We recognize that differences in Zn/Co metabolism due to adaptation to differences in dMn concentration in the field may exist in diatoms. However, we find no major difference in the NE Pacific diatom Mn quotas in comparison to those of Atlantic *T. pseudonana.* Furthermore, unlike the notably high dCo concentrations observed at Line P, surface dMn concentrations demonstrated typical scavenged-like profiles with offshore surface maxima of ~4 nM as observed previously in the north Pacific (Landing and Bruland 1980, 1987). We therefore find no evidence of novel Mn metabolism in the NE Pacific diatoms in this study, despite their apparent adaptation to high dCo.

We have demonstrated that the Atlantic diatoms *T. pseudonana* and *P. tricornutum* are capable of growth using Co in place of Zn when limited for Zn, but at the cost of reduction in growth rate. In contrast, the NE Pacific diatoms *Thalassiosira* UNC1203 and *P. delicatissima* do not exhibit this growth rate reduction (Fig. 5). We suggest that these observations are linked to the higher surface dCo:dZn ratios found in the NE Pacific waters from which *Thalassiosira* UNC1203 and *P. delicatissima* were isolated. Measurements of dZn and dCo concentrations at stations P1-P8 taken on the GeoMICS expedition (Fig. 1a) revealed surprisingly high dCo:dZn ratios at the surface (<100 m) across all sampled stations, which ranged from 0.03:1 – 3.52:1 (Fig. 2). Prior studies have found similarly low surface dZn concentrations in the subarctic Northeast Pacific (Bruland et al. 1978; Martin et al. 1989; Lohan et al. 2002). As global average dCo concentrations range from $50 - 100$ pmol L^{-1} (Tagliabue et al. 2018), maximum surface dCo:dZn ratios are typically ~0.4:1 (Martin et al. 1989). However, we observed surface dCo

31

exceeding 150 pmol L^{-1} at multiple stations, resulting in dCo:dZn ratios reaching as high as 3.52:1 at surface (0 – 100m) depths (Fig. 2b, Table 1). To our knowledge, this is the first observation of dCo abundance exceeding dZn. Comparison with dCo:dZn ratios from two GEOTRACES expeditions, the Eastern Pacific (EPZT) and North Atlantic (NAZT), revealed how anomalously high the surface dCo:dZn ratios from the NE Pacific near Line P were (Fig. 4). Among the diatoms studied, *Thalassiosira* UNC1203 and *P. delicatissima* are therefore unique in that they were isolated from an environment with high surface dCo:dZn ratios (Table 1). In this context, the enhanced growth rates of *Thalassiosira* UNC1203 in Co amended media and the highly efficient Zn/Co metabolic substitution ability observed in *P. delicatissima* may be related to the high dCo:dZn surface ratios of their native environment.

It is important to note that both *Thalassiosira* UNC1203 and *P. delicatissima* UNC1205, isolated from station P8 of Line P, are offshore isolates. This station is dominated by small celled phytoplankton such as *Synechococcus* spp. and is likely limited by Fe (Ribalet et al. 2010) and potentially by Zn given the high dCo:dZn ratios measured in this study. The ability to metabolically substitute Zn for Co may therefore benefit these diatoms if trace metal nutrient depletion leads to selection pressure for biochemical flexibility (Saito and Goepfert 2008). In contrast, the strains of *T. pseudonana* and *P. tricornutum* used in this study are coastal isolates (Table 1). It has been hypothesized that an intense drawdown of macronutrients and trace metals during bloom conditions in these nearshore environments would again lead to selection pressure, giving those species with a Zn/Co substitution ability an advantage (Saito and Goepfert 2008). A

32

growth advantage given by a Zn/Co substitution ability may therefore explain its presence in the coastal diatoms *T. pseudonana* and *P. tricornutum*. Zn/Co substitution is thus a useful metabolic ability for organisms occupying both offshore and coastal environments. The higher surface dCo:dZn ratios observed in the NE Pacific (Table 1, Fig. 2b) suggest that this ability is optimized for Co use in the NE Pacific. The Zn:Co quotas of single diatom cells measured across four stations of Line P were consistently about ~250 mol:mol at stations P3 – P8 (Fig. 10c), demonstrating a high Zn demand that was consistent with measured pZn:pCo ratios of ~ 25:1 (Fig. 2c). Our culture data suggests that, should this high Zn demand become difficult to fulfill due to intense Zn drawdown, diatoms capable of Zn/Co substitution would have a selection advantage as they are able to efficiently use Co in place of Zn.

The concentration of added Zn or Co at which maximum growth rates were achieved varied among these diatoms, implying unique chemical niches. The genera *Thalassiosira* and *Pseudo-nitzschia* are known to be highly abundant and widely distributed in nature. The worldwide distribution of these genera encompasses different ribotypes, suggesting that these diatoms have evolved to diversify to varying environmental conditions (Malviya et al. 2016). In this context, Zn/Co metabolic substitution is likely a means by which diatoms are able exploit a wide range of ecological and chemical niches.

We have shown that the degree to which Co can nutritionally compensate for Zn as assessed by growth rate varies among these diatom species, with Co partially restoring growth rates in the Atlantic diatoms *T. pseudonana* and *P. tricornutum*, and completely restoring growth

33

rates in the NE Pacific diatoms *Thalassiosira* UNC1203 and *P. delicatissima.* We suggest that the difference between Co partially versus fully restoring growth rate is related to differences in substitution efficiency— that is, how well Co^{2+} maintains enzyme activity compared to Zn^{2+}. Coordination chemistry on the amino acid—metal interaction level of Zn^{2+} and Co^{2+} at the active site of cambialistic metalloenzymes, such as the Zn^{2+}/Co^{2+} carbonic anhydrase TWCA1, will be key to understanding this. Moreover, as TWCA1 is widely distributed in many marine eukaryotic photosynthetic organisms beyond diatoms (Morel et al. in revision), the extent of Zn/Co cambialism is likely taxonomically widespread among marine phytoplankton.

In this manuscript, we present evidence of a metabolic Zn/Co substitution ability in the diatoms *T. pseudonana* CCMP1335*, P. tricornutum* CCMP632, *Thalassiosira* UNC1203, and *P. delicatissima* UNC1205. Enhanced growth rates of the NE Pacific diatoms *Thalassiosira* UNC1203 and *P. delicatissima* with Co additions are likely related to the relatively dCo-rich surface environment they were isolated from. Confirming previous findings, we observed that *T. pseudonana* attains higher maximum growth rates with Zn nutrition while Co additions achieve only ~50% of this maximum (Sunda and Huntsman 1995). *P. tricornutum* similarly attains higher maximum growth rates with Zn compared to Co nutrition, thus Co-based metabolism is possible for both Atlantic diatoms but at the cost of growth rate reduction. We find that the ability to metabolically substitute Co in place of Zn in *P. delicatissima* is the most efficient of all species in this study in terms of growth rate, although the biochemical basis for this is unknown.

34

We conclude that the efficiency of metabolic Zn/Co substitution is a species-specific and important chemical niche in marine diatoms and other marine eukaryotic phototrophs.

References

Ahlgren, N. A., A. Noble, A. P. Patton, and others. 2014. The unique trace metal and mixed layer conditions of the costa rica upwelling dome support a distinct and dense community of Synechococcus. Limnol. Oceanogr. doi:10.4319/lo.2014.59.6.2166

Alscher, R. G., N. Erturk, and L. S. Heath. 2002. Role of superoxide dismutases (SODs) in controlling oxidative stress in plants. *Journal of Experimental Botany*.

Aristilde, L., Y. Xu, and F. M. M. Morel. 2012. Weak organic ligands enhance zinc uptake in marine phytoplankton. Environ. Sci. Technol. doi:10.1021/es300335u

Armbrust, E. V. 2009. The life of diatoms in the world's oceans. Nature.

doi:10.1038/nature08057

Berger, C. J. M., S. M. Lippiatt, M. G. Lawrence, and K. W. Bruland. 2008. Application of a chemical leach technique for estimating labile particulate aluminum, iron, and manganese in the Columbia River plume and coastal waters off Oregon and Washington. J. Geophys. Res. doi:10.1029/2007jc004703

Biller, D. V., and K. W. Bruland. 2013. Sources and distributions of Mn, Fe, Co, Ni, Cu, Zn, and Cd relative to macronutrients along the central California coast during the spring and summer upwelling season. Mar. Chem. doi:10.1016/j.marchem.2013.06.003

Bowie, A. R., D. J. Whitworth, E. P. Achterberg, R. F. C. Mantoura, and P. J. Worsfold. 2002. Biogeochemistry of Fe and other trace elements (Al, Co, Ni) in the upper Atlantic Ocean. Deep. Res. Part I Oceanogr. Res. Pap. doi:10.1016/S0967-0637(01)00061-9

Bruland, K. W. 1989. Complexation of zinc by natural organic ligands in the central North Pacific. Limnol. Oceanogr. **34**: 269–285. doi:10.4319/lo.1989.34.2.0269

Bruland, K. W., G. A. Knauer, and J. H. Martin. 1978. Zinc in north-east Pacific water. Nature **271**: 741–743. doi:10.1038/271741a0

Bruland, K. W., and M. C. Lohan. 2003. Controls of Trace Metals in Seawater, p. 23–47. *In* Treatise on Geochemistry. Elsevier.

Coale, K. H. 1991. Effects of iron, manganese, copper, and zinc enrichments on productivity and biomass in the subarctic Pacific. Limnol. Oceanogr. doi:10.4319/lo.1991.36.8.1851

Colman, B., and C. Rotatore. 1995. Photosynthetic inorganic carbon uptake and accumulation in

two marine diatoms. Plant Cell Environ. doi:10.1111/j.1365-3040.1995.tb00601.x

Cowen, J. P., and K. W. Bruland. 1985. Metal deposits associated with bacteria: implications for Fe and Mn marine biogeochemistry. Deep Sea Res. Part A, Oceanogr. Res. Pap. doi:10.1016/0198-0149(85)90078-0

Crawford, D. W., M. S. Lipsen, D. A. Purdie, and others. 2003. Influence of zinc and iron enrichments on phytoplankton growth in the northeastern subarctic Pacific. Limnol. Oceanogr. doi:10.4319/lo.2003.48.4.1583

Cummins, P. F., and T. Ross. 2020. Secular trends in water properties at Station P in the northeast Pacific: an updated analysis. Prog. Oceanogr. 102329. doi:10.1016/j.pocean.2020.102329

Cutter, G. A., and K. W. Bruland. 2012. Rapid and noncontaminating sampling system for trace elements in global ocean surveys. Limnol. Oceanogr. Methods. doi:10.4319/lom.2012.10.425

DiMario, R. J., M. C. Machingura, G. L. Waldrop, and J. V. Moroney. 2018. The many types of carbonic anhydrases in photosynthetic organisms. Plant Sci. doi:10.1016/j.plantsci.2017.12.002

Donat, J. R., and K. W. Bruland. 1990. A comparison of two voltammetric techniques for determining zinc speciation in Northeast Pacific Ocean waters. Mar. Chem. doi:10.1016/0304-4203(90)90050-M

Dyhrman, S. T., and K. C. Ruttenberg. 2006. Presence and regulation of alkaline phosphatase

activity in eukaryotic phytoplankton from the coastal ocean: Implications for dissolved organic phosphorus remineralization. Limnol. Oceanogr. doi:10.4319/lo.2006.51.3.1381

Ellwood, M. J., and C. M. G. van den Berg. 2000. Zinc speciation in the Northeastern Atlantic Ocean. Mar. Chem. doi:10.1016/S0304-4203(99)00085-7

Hawco, N. J., P. J. Lam, J. M. Lee, D. C. Ohnemus, A. E. Noble, N. J. Wyatt, M. C. Lohan, and M. A. Saito. 2018. Cobalt scavenging in the mesopelagic ocean and its influence on global mass balance: Synthesizing water column and sedimentary fluxes. Mar. Chem. doi:10.1016/j.marchem.2017.09.001

Hawco, N. J., D. C. Ohnemus, J. A. Resing, B. S. Twining, and M. A. Saito. 2016. A dissolved cobalt plume in the oxygen minimum zone of the eastern tropical South Pacific. Biogeosciences. doi:10.5194/bg-13-5697-2016

Hawco, N. J., and M. A. Saito. 2018. Competitive inhibition of cobalt uptake by zinc and manganese in a pacific Prochlorococcus strain: Insights into metal homeostasis in a streamlined oligotrophic cyanobacterium. Limnol. Oceanogr. doi:10.1002/lno.10935

Hillebrand, H., C. D. Dürselen, D. Kirschtel, U. Pollingher, and T. Zohary. 1999. Biovolume calculation for pelagic and benthic microalgae. J. Phycol. doi:10.1046/j.1529-8817.1999.3520403.x

Intwala, A., T. D. Patey, D. M. Polet, and M. R. Twiss. 2008. Nutritive substitution of zinc by cadmium and cobalt in phytoplankton isolated from the lower Great Lakes. J. Great Lakes Res. doi:10.3394/0380-1330(2008)34[1:NSOZBC]2.0.CO;2

Irving, B. H., and R. J. P. Williams. 1953. The Stability of Transition-metal Complexes. J. Chem. Soc. doi:10.1039/JR9530003192

Jakuba, R. W., J. W. Moffett, and S. T. Dyhrman. 2008. Evidence for the linked biogeochemical cycling of zinc, cobalt, and phosphorus in the western North Atlantic Ocean. Global Biogeochem. Cycles **22**: n/a-n/a. doi:10.1029/2007GB003119

Jakuba, R. W., M. A. Saito, J. W. Moffett, and Y. Xu. 2012. Dissolved zinc in the subarctic North Pacific and Bering Sea: Its distribution, speciation, and importance to primary producers. Global Biogeochem. Cycles. doi:10.1029/2010GB004004

Jensen, E. L., R. Clement, A. Kosta, S. C. Maberly, and B. Gontero. 2019. A new widespread subclass of carbonic anhydrase in marine phytoplankton. ISME J. doi:10.1038/s41396-019-0426-8

Johnson, K. S., E. Boyle, K. Bruland, and others. 2007. Developing standards for dissolved iron in seawater. Eos (Washington. DC). doi:10.1029/2007EO110003

Klug, A. 2010. The Discovery of Zinc Fingers and Their Applications in Gene Regulation and Genome Manipulation. Annu. Rev. Biochem. doi:10.1146/annurev-biochem-010909-095056

Knauer, G. A., J. H. Martin, and R. M. Gordon. 1982. Cobalt in north-east Pacific waters. Nature. doi:10.1038/297049a0

Koch, F., and S. Trimborn. 2019. Limitation by fe, zn, co, and b12 results in similar physiological responses in two antarctic phytoplankton species. Front. Mar. Sci.

40

doi:10.3389/fmars.2019.00514

Landing, W. M., and K. W. Bruland. 1980. Manganese in the North Pacific. Earth Planet. Sci. Lett. doi:10.1016/0012-821X(80)90149-1

Landing, W. M., and K. W. Bruland. 1987. The contrasting biogeochemistry of iron and manganese in the Pacific Ocean. Geochim. Cosmochim. Acta. doi:10.1016/0016-7037(87)90004-4

Lane, T. W., M. A. Saito, G. N. George, I. J. Pickering, R. C. Prince, and F. M. M. Morel. 2005. A cadmium enzyme from a marine diatom. Nature **435**: 42–42. doi:10.1038/435042a

Lee, J. G., and F. M. M. Morel. Replacement of zinc by cadmium in marine phytoplankton. Mar. Ecol. Prog. Ser. **127**: 305–309. doi:10.2307/24855143

Lohan, M. C., P. J. Statham, and D. W. Crawford. 2002. Total dissolved zinc in the upper water column of the subarctic North East Pacific. Deep. Res. Part II Top. Stud. Oceanogr. doi:10.1016/S0967-0645(02)00215-1

Malviya, S., E. Scalco, S. Audic, and others. 2016. Insights into global diatom distribution and diversity in the world's ocean. Proc. Natl. Acad. Sci. U. S. A. **113**: E1516-25. doi:10.1073/pnas.1509523113

Martin, J. H., R. M. Gordon, S. Fitzwater, and W. W. Broenkow. 1989. Vertex: phytoplankton/iron studies in the Gulf of Alaska. Deep Sea Res. Part A, Oceanogr. Res. Pap. **36**: 649–680. doi:10.1016/0198-0149(89)90144-1

Matsuda, Y., T. Hara, and B. Colman. 2001. Regulation of the induction of bicarbonate uptake

by dissolved CO2 in the marine diatom, Phaeodactylum tricornutum. Plant, Cell Environ. doi:10.1046/j.1365-3040.2001.00702.x

Menden-Deuer, S., and E. J. Lessard. 2000. Carbon to volume relationships for dinoflagellates, diatoms, and other protist plankton. Limnol. Oceanogr. doi:10.4319/lo.2000.45.3.0569

Moffett, J. W., and J. Ho. 1996. Oxidation of cobalt and manganese in seawater via a common microbially catalyzed pathway. Geochim. Cosmochim. Acta. doi:10.1016/0016-7037(96)00176-7

Morel, F. M. M., J. R. Reinfelder, S. B. Roberts, C. P. Chamberlain, J. G. Lee, and D. Yee. 1994. Zinc and carbon co-limitation of marine phytoplankton. Nature **369**: 740–742. doi:10.1038/369740a0

Noble, A. E., C. H. Lamborg, D. C. Ohnemus, and others. 2012. Basin-scale inputs of cobalt, iron, and manganese from the Benguela-Angola front to the South Atlantic Ocean. Limnol. Oceanogr. doi:10.4319/lo.2012.57.4.0989

Noble, A. E., D. C. Ohnemus, N. J. Hawco, P. J. Lam, and M. A. Saito. 2017. Coastal sources, sinks and strong organic complexation of dissolved cobalt within the US North Atlantic GEOTRACES transect GA03. Biogeosciences. doi:10.5194/bg-14-2715-2017

Noble, A. E., M. A. Saito, K. Maiti, and C. R. Benitez-Nelson. 2008. Cobalt, manganese, and iron near the Hawaiian Islands: A potential concentrating mechanism for cobalt within a cyclonic eddy and implications for the hybrid-type trace metals. Deep. Res. Part II Top. Stud. Oceanogr. doi:10.1016/j.dsr2.2008.02.010

Nolting, R. F., M. Heijne, J. T. de Jong, K. R. Timmermans, and H. J. de Baar. 2000. The determination and distribution of Zn in surface water samples collected in the northeast Atlantic Ocean. J. Environ. Monit. **2**: 534–8.

Ohnemus, D. C., M. E. Auro, R. M. Sherrell, M. Lagerström, P. L. Morton, B. S. Twining, S. Rauschenberg, and P. J. Lam. 2014. Laboratory intercomparison of marine particulate digestions including Piranha: A novel chemical method for dissolution of polyethersulfone filters. Limnol. Oceanogr. Methods. doi:10.4319/lom.2014.12.530

Price, N. M., and F. M. M. Morel. 1990. Cadmium and cobalt substitution for zinc in a marine diatom. Nature. doi:10.1038/344658a0

Rauschenberg, S., and B. S. Twining. 2015. Evaluation of approaches to estimate biogenic particulate trace metals in the ocean. Mar. Chem. doi:10.1016/j.marchem.2015.01.004

Ribalet, F., A. Marchetti, K. A. Hubbard, and others. 2010. Unveiling a phytoplankton hotspot at a narrow boundary between coastal and offshore waters. Proc. Natl. Acad. Sci. U. S. A. **107**: 16571–6. doi:10.1073/pnas.1005638107

Riebesell, U., D. A. Wolf-Gladrow, and V. Smetacek. 1993. Carbon dioxide limitation of marine phytoplankton growth rates. Nature. doi:10.1038/361249a0

Roberts, K., E. Granum, R. C. Leegood, and J. A. Raven. 2007. Carbon acquisition by diatoms. Photosynth. Res. doi:10.1007/s11120-007-9172-2

Saito, M. A., and T. J. Goepfert. 2008. Zinc-cobalt colimitation of *Phaeocystis antarctica*. Limnol. Oceanogr. **53**: 266–275. doi:10.4319/lo.2008.53.1.0266

Saito, M. A., M. R. McIlvin, D. M. Moran, T. J. Goepfert, G. R. DiTullio, A. F. Post, and C. H. Lamborg. 2014. Multiple nutrient stresses at intersecting Pacific Ocean biomes detected by protein biomarkers. Science (80-.). doi:10.1126/science.1256450

Saito, M. A., and J. W. Moffett. 2001. Complexation of cobalt by natural organic ligands in the Sargasso sea as determined by a new high-sensitivity electrochemical cobalt speciation method suitable for open ocean work. Mar. Chem. doi:10.1016/S0304-4203(01)00025-1

Saito, M. A., and J. W. Moffett. 2002. Temporal and spatial variability of cobalt in the Atlantic Ocean. Geochim. Cosmochim. Acta. doi:10.1016/S0016-7037(02)00829-3

Saito, M. A., J. W. Moffett, S. W. Chisholm, and J. B. Waterbury. 2002. Cobalt limitation and uptake in *Prochlorococcus*. Limnol. Oceanogr. **47**: 1629–1636. doi:10.4319/lo.2002.47.6.1629

Saito, M. A., J. W. Moffett, and G. R. DiTullio. 2004. Cobalt and nickel in the Peru upwelling region: A major flux of labile cobalt utilized as a micronutrient. Global Biogeochem. Cycles. doi:10.1029/2003GB002216

Saito, M. A., A. E. Noble, N. Hawco, and others. 2017. The acceleration of dissolved cobalt's ecological stoichiometry due to biological uptake, remineralization, and scavenging in the Atlantic Ocean. Biogeosciences. doi:10.5194/bg-14-4637-2017

Saito, M. A., and D. L. Schneider. 2006. Examination of precipitation chemistry and improvements in precision using the Mg(OH)2 preconcentration inductively coupled plasma mass spectrometry (ICP-MS) method for high-throughput analysis of open-ocean Fe

44

and Mn in seawater. Anal. Chim. Acta. doi:10.1016/j.aca.2006.02.028

Saito, M. A., D. M. Sigman, and F. M. M. Morel. 2003. The bioinorganic chemistry of the ancient ocean: The co-evolution of cyanobacterial metal requirements and biogeochemical cycles at the Archean-Proterozoic boundary? Inorganica Chim. Acta. doi:10.1016/S0020-1693(03)00442-0

Schlitzer, R. 2011. Ocean Data View User's Guide. Contract.

Shaked, Y., Y. Xu, K. Leblanc, and F. M. M. Morel. 2006. Zinc availability and alkaline phosphatase activity in Emiliania huxleyi: Implications for Zn-P co-limitation in the ocean. Limnol. Oceanogr. doi:10.4319/lo.2006.51.1.0299

Sim, N., and K. J. Orians. 2019. Annual variability of dissolved manganese in Northeast Pacific along Line-P: 2010–2013. Mar. Chem. doi:10.1016/j.marchem.2019.103702

Sunda, W. G., and S. A. Huntsman. 1995. Cobalt and zinc interreplacement in marine phytoplankton: Biological and geochemical implications. Limnol. Oceanogr. **40**: 1404–1417. doi:10.4319/lo.1995.40.8.1404

Sunda, W. G., and S. A. Huntsman. 1996. Antagonisms between cadmium and zinc toxicity and manganese limitation in a coastal diatom. Limnol. Oceanogr. doi:10.4319/lo.1996.41.3.0373

Sunda, W. G., and S. A. Huntsman. 1998. Interactive effects of external manganese, the toxic metals copper and zinc, and light in controlling cellular manganese and growth in a coastal diatom. Limnol. Oceanogr. doi:10.4319/lo.1998.43.7.1467

Sunda, W. G., and S. A. Huntsman. 2000. Effect of Zn, Mn, and Fe on Cd accumulation in phytoplankton: Implications for oceanic Cd cycling. Limnol. Oceanogr. doi:10.4319/lo.2000.45.7.1501

Sunda, W. G., N. M. Price, and F. M. M. Morel. 2005. Trace Metal Ion Buffers and Their Use in Culture Studies, *In* Algal Culturing Techniques.

Sundby, B., L. G. Anderson, P. O. J. Hall, Å. Iverfeldt, M. M. R. van der Loeff, and S. F. G. Westerlund. 1986. The effect of oxygen on release and uptake of cobalt, manganese, iron and phosphate at the sediment-water interface. Geochim. Cosmochim. Acta. doi:10.1016/0016-7037(86)90411-4

Swanner, E. D., N. J. Planavsky, S. V. Lalonde, and others. 2014. Cobalt and marine redox evolution. Earth Planet. Sci. Lett. doi:10.1016/j.epsl.2014.01.001

Tagliabue, A., N. J. Hawco, R. M. Bundy, W. M. Landing, A. Milne, P. L. Morton, and M. A. Saito. 2018. The Role of External Inputs and Internal Cycling in Shaping the Global Ocean Cobalt Distribution: Insights From the First Cobalt Biogeochemical Model. Global Biogeochem. Cycles. doi:10.1002/2017GB005830

Timmermans, K. R., J. Snoek, L. J. A. Gerringa, I. Zondervan, and H. J. W. de Baar. 2001. Not all eukaryotic algae can replace zinc with cobalt: Chaetoceros calcitrans (Bacillariophyceae) versus Emiliania huxleyi (Prymnesiophyceae). Limnol. Oceanogr. **46**: 699–703. doi:10.4319/lo.2001.46.3.0699

Twining, B. S., and S. B. Baines. 2013. The Trace Metal Composition of Marine Phytoplankton.

Ann. Rev. Mar. Sci. doi:10.1146/annurev-marine-121211-172322

Twining, B. S., S. B. Baines, J. B. Bozard, S. Vogt, E. A. Walker, and D. M. Nelson. 2011. Metal quotas of plankton in the equatorial Pacific Ocean. Deep. Res. Part II Top. Stud. Oceanogr. doi:10.1016/j.dsr2.2010.08.018

Twining, B. S., S. B. Baines, N. S. Fisher, J. Maser, S. Vogt, C. Jacobsen, A. Tovar-Sanchez, and S. A. Sañudo-Wilhelmy. 2003. Quantifying trace elements in individual aquatic protist cells with a synchrotron X-ray fluorescence microprobe. Anal. Chem. doi:10.1021/ac034227z

Twining, B. S., S. Rauschenberg, P. L. Morton, D. C. Ohnemus, and P. J. Lam. 2015. Comparison of particulate trace element concentrations in the North Atlantic Ocean as determined with discrete bottle sampling and in situ pumping. Deep. Res. Part II Top. Stud. Oceanogr. doi:10.1016/j.dsr2.2014.11.005

Vance, D., G. F. de Souza, Y. Zhao, J. T. Cullen, and M. C. Lohan. 2019. The relationship between zinc, its isotopes, and the major nutrients in the North-East Pacific. Earth Planet. Sci. Lett. doi:10.1016/j.epsl.2019.115748

Vogt, S. 2003. MAPS: A set of software tools for analysis and visualization of 3D X-ray fluorescence data sets. *Journal De Physique. IV : JP*.

Waldron, K. J., J. C. Rutherford, D. Ford, and N. J. Robinson. 2009. Metalloproteins and metal sensing. Nature **460**: 823–830. doi:10.1038/nature08300

Wu, J., and E. A. Boyle. 1998. Determination of iron in seawater by high-resolution isotope

dilution inductively coupled plasma mass spectrometry after Mg(OH)2 coprecipitation. Anal. Chim. Acta. doi:10.1016/S0003-2670(98)00145-7

Xu, Y., D. Tang, Y. Shaked, and F. M. M. Morel. 2007. Zinc, cadmium, and cobalt interreplacement and relative use efficiencies in the coccolithophore Emiliania huxleyi. Limnol. Oceanogr. doi:10.4319/lo.2007.52.5.2294

Yee, D., and F. M. M. Morel. 1996. In vivo substitution of zinc by cobalt in carbonic anhydrase of a marine diatom. Limnol. Oceanogr. doi:10.4319/lo.1996.41.3.0573

Young, J. N., A. M. C. Heureux, R. E. Sharwood, R. E. M. Rickaby, F. M. M. Morel, and S. M. Whitney. 2016. Large variation in the Rubisco kinetics of diatoms reveals diversity among their carbon-concentrating mechanisms. J. Exp. Bot. doi:10.1093/jxb/erw163

Zheng, L., T. Minami, W. Konagaya, C. Y. Chan, M. Tsujisaka, S. Takano, K. Norisuye, and Y. Sohrin. 2019. Distinct basin-scale-distributions of aluminum, manganese, cobalt, and lead in the North Pacific Ocean. Geochim. Cosmochim. Acta. doi:10.1016/j.gca.2019.03.038

Tables

Table 1. Diatoms used in this study and observed concentration ranges of total dissolved surface

(0-30 m) Zn and Co.

Diatom	Location of Isolation	Geographical Context	Surface dCo	Surface dZn	dCo:dZn (M:M)
Thalassiosira pseudonana CCMP1335	Moriches Bay, Long Island, New York	Northwest Atlantic Ocean	59.9 – 133 pmol L^{-1} (1,2)	1.32 nmol L^{-1} (1)	0.05:1 – 0.10:1
Phaeodactylum tricornutum CCMP632	Blackpool, England, British Isles	Northeast Atlantic Ocean	53.6 – 98.2 pmol L^{-1} (3)	0.5 – 1.5 nmol L^{-1} (4,5)	0.07:1 – 0.11:1
Thalassiosira sp UNC1203	Station P8, Line P transect	Northeast Pacific Ocean	39 – 389 pmol L^{-1} (6)	0.03 – 0.65 nmol L^{-1} (6)	0.2:1 – 3.52:1
Pseudo-nitzschia delicatissima UNC1205	Station P8, Line P transect	Northeast Pacific Ocean	39 – 389 pmol L^{-1} (6)	0.03 – 0.65 nmol L^{-1} (6)	0.2:1 – 3.52:1

Table 1 references:
1. (Jakuba et al. 2008)
2. (Saito and Moffett 2002)
3. (Bowie et al. 2002)
4. (Ellwood and van den Berg 2000)
5. (Nolting et al. 2000)
6. This study

Table 2. Growth rates of *Thalassiosira pseudonana* CCMP1335 in Zn and Co simple limitation (one element varies) and matrix (both elements covaried) treatments. Simple limitation was conducted in duplicate (replicates A and B). Metal concentrations are provided as the amount of metal added to each media treatment ("Added [M]" column), the total metal concentration (background media concentration + added concentration, "Total [M]*" column), and the concentration of free metal ions calculated using the total metal concentration and media composition ("log[M^{2+}]" columns). Average growth rates are given $\pm$ the standard deviation of duplicate growth rates. NA refers to not available. Biomass yield is reported as relative fluorescent units (RFU).

Experiment Type	Added [Zn] (nM)	Added [Co] (nM)	Total [Zn]* (nM)	Total [Co]* (nM)	log[Zn^{2+}] (M)	log[Co^{2+}] (M)	Growth rate replicate A	Growth rate replicate B	Growth rate average (d^{-1})	Yield (Maximum RFU)
Simple	0	0	0.9	0.1	-13.04	-13.63	0	0	0	1.8
Simple	1	0	1.9	0.1	-12.71	-13.63	0.23	NA	0.23	27.2
Simple	3	0	3.9	0.1	-12.40	-13.63	0.28	0.37	0.33 ± 0.06	97.2
Simple	10	0	10.9	0.1	-11.95	-13.63	0.57	0.65	0.61 ± 0.06	235.8
Simple	30	0	30.9	0.1	-11.50	-13.63	0.69	0.74	0.72 ± 0.03	276.4
Simple	100	0	100.9	0.1	-10.99	-13.63	0.65	0.72	0.69 ± 0.05	229.5
Simple	0	1	0.9	1.1	-13.04	-12.59	0.13	0.23	0.18 ± 0.07	17.8
Simple	0	3	0.9	3.1	-13.04	-12.14	0.23	0.30	0.27 ± 0.05	26.9
Simple	0	10	0.9	10.1	-13.04	-11.63	0.38	0.38	0.38 ± 0.003	78.4
Simple	0	30	0.9	30.1	-13.04	-11.15	0.38	0.32	0.35 ± 0.04	76.2
Matrix	1	1	1.9	1.1	-12.71	-12.59	0.28	NA	0.28	9.1
Matrix	3	1	3.9	1.1	-12.40	-12.59	0.36	NA	0.36	46.7
Matrix	10	1	10.9	1.1	-11.95	-12.59	0.67	NA	0.67	144.7
Matrix	100	1	100.9	1.1	-10.99	-12.59	0.82	NA	0.82	221.6
Matrix	1	3	1.9	3.1	-12.71	-12.14	0.49	NA	0.49	81.5
Matrix	3	3	3.9	3.1	-12.40	-12.14	0.49	NA	0.49	94.3
Matrix	10	3	10.9	3.1	-11.95	-12.14	0.66	NA	0.66	207.1

50

Experiment Type	Added [Zn] (nM)	Added [Co] (nM)	Total [Zn]* (nM)	Total [Co]* (nM)	$\log[Zn^{2+}]$ (M)	$\log[Co^{2+}]$ (M)	Growth rate replicate A	Growth rate replicate B	Growth rate average (d^{-1})	Yield (Maximum RFU)
Matrix	30	3	30.9	3.1	-11.50	-12.14	0.77	NA	0.77	213.8
Matrix	1	10	1.9	10.1	-12.71	-11.63	0.67	NA	0.67	184.0
Matrix	3	10	3.9	10.1	-12.40	-11.63	0.59	NA	0.59	234.4
Matrix	10	10	10.9	10.1	-11.95	-11.63	0.68	NA	0.68	215.5
Matrix	100	10	100.9	10.1	-10.99	-11.63	0.80	NA	0.80	237.2
Matrix	3	30	3.9	30.1	-12.40	-11.15	0.62	NA	0.62	166.7
Matrix	30	30	30.9	30.1	-11.50	-11.15	0.65	NA	0.65	223.0
Matrix	1	100	1.9	100.1	-12.71	-10.63	0.65	NA	0.65	187.7
Matrix	3	100	3.9	100.1	-12.40	-10.63	0.65	NA	0.65	218.5
Matrix	10	100	10.9	100.1	-11.95	-10.63	0.62	NA	0.62	215.5
Matrix	30	100	30.9	100.1	-11.50	-10.63	0.69	NA	0.69	209.6
Matrix	100	100	100.9	100.1	-10.99	-10.63	0.65	NA	0.65	306.4

Table 3. Growth rates of *Phaeodactylum tricornutum* CCMP632 in Zn and Co simple limitation (one element varies) and matrix (both elements covaried) treatments. Simple limitation was conducted in duplicate (replicates A and B). Metal concentrations are provided as the amount of metal added to each media treatment ("Added [M]" column), the total metal concentration (background media concentration + added concentration, "Total [M]*" column), and the concentration of free metal ions calculated using the total metal concentration and media composition ("log[M^{2+}]" columns). Average growth rates are given ± the standard deviation of duplicate growth rates. NA refers to not available. Biomass yield is reported as relative fluorescent units (RFU).

Experiment Type	Added [Zn] (nM)	Added [Co] (nM)	Total [Zn]* (nM)	Total [Co]* (nM)	$\log[Zn^{2+}]$ (M)	$\log[Co^{2+}]$ (M)	Growth rate replicate A	Growth rate replicate B	Growth rate average (d^{-1})	Yield (Maximum RFU)
Simple	0	0	0.9	0.1	-13.04	-13.63	0.60	NA	0.60	116.1
Simple	0.1	0	1	0.1	-12.99	-13.63	0.60	0.63	0.62 ± 0.02	136.5
Simple	1	0	1.9	0.1	-12.71	-13.63	0.61	0.73	0.67 ± 0.08	93.8
Simple	3	0	3.9	0.1	-12.40	-13.63	0.67	0.67	0.67 ± 0	134.8
Simple	10	0	10.9	0.1	-11.95	-13.63	0.79	0.82	0.80 ± 0.02	279.0
Simple	30	0	30.9	0.1	-11.50	-13.63	0.80	0.80	0.80 ± 0	239.2
Simple	100	0	100.9	0.1	-10.99	-13.63	0.78	0.81	0.80 ± 0.02	300.2
Simple	0	0.1	0.9	0.2	-13.04	-13.33	0.56	0.45	0.51 ± 0.08	78.2
Simple	0	3	0.9	3.1	-13.04	-12.14	0.48	0.52	0.50 ± 0.03	75.9
Simple	0	10	0.9	10.1	-13.04	-11.63	0.61	0.58	0.59 ± 0.02	112.4

51

Experiment Type	Added [Zn] (nM)	Added [Co] (nM)	Total [Zn]* (nM)	Total [Co]* (nM)	log[Zn^{2+}] (M)	log[Co^{2+}] (M)	Growth rate replicate A	Growth rate replicate B	Growth rate average (d^{-1})	Yield (Maximum RFU)
Simple	0	30	0.9	30.1	-13.04	-11.15	0.62	0.59	0.61 ± 0.03	118.7
Simple	0	100	0.9	100.1	-13.04	-10.63	0.71	NA	0.71	157.7
Matrix	100	100	100.9	100.1	-10.99	-10.63	0.92	0.89	0.90 ± 0.02	138.7
Matrix	30	30	30.9	30.1	-11.50	-11.15	0.90	0.93	0.91 ± 0.02	130.3
Matrix	10	10	10.9	10.1	-11.95	-11.63	0.89	0.86	0.88 ± 0.02	137.9
Matrix	100	10	100.9	10.1	-10.99	-11.63	0.85	0.81	0.83 ± 0.03	111.3
Matrix	10	100	10.9	100.1	-11.95	-10.63	0.83	0.71	0.77 ± 0.08	138.6
Matrix	30	3	30.9	3.1	-11.50	-12.14	0.81	0.83	0.82 ± 0.01	132.3
Matrix	3	30	3.9	30.1	-12.40	-11.15	0.96	0.84	0.90 ± 0.09	142.9
Matrix	1	100	1.9	100.1	-12.71	-10.63	0.79	NA	0.79	122.2
Matrix	100	1	100.9	1.1	-10.99	-12.59	0.90	0.86	0.88 ± 0.03	148.8

Table 4. Growth rates of NE Pacific *Thalassiosira* UNC1203 in Zn and Co simple limitation (one element varies) and matrix (both elements covaried) treatments. Simple limitation was conducted in duplicate (replicates A and B). Metal concentrations are provided as the amount of metal added to each media treatment ("Added [M]" column), the total metal concentration (background media concentration + added concentration, "Total [M]*" column), and the concentration of free metal ions calculated using the total metal concentration and media composition ("log[M^{2+}]" columns). Average growth rates are given ± the standard deviation of duplicate growth rates. NA refers to not available. Biomass yield is reported as relative fluorescent units (RFU).

Experiment Type	Added [Zn] (nM)	Added [Co] (nM)	Total [Zn]* (nM)	Total [Co]* (nM)	log[Zn^{2+}] (M)	log[Co^{2+}] (M)	Growth rate replicate A	Growth rate replicate B	Growth rate average (d^{-1})	Yield (Maximum RFU)
Simple	0	0	0.9	0.1	-13.04	-13.63	0.01	0.03	0.02 ± 0.01	2.9
Simple	1	0	1.9	0.1	-12.71	-13.63	0.01	0.04	0.02 ± 0.02	3.6
Simple	3	0	3.9	0.1	-12.40	-13.63	NA	0.01	0.01	2.7
Simple	10	0	10.9	0.1	-11.95	-13.63	0.02	0.02	0.02 ± 0.005	3.0
Simple	30	0	30.9	0.1	-11.50	-13.63	0.06	0.12	0.09 ± 0.04	7.2

Simple	100	0	100.9	0.1	-10.99	-13.63	0.29	0.30	0.30 ± 0.01	35.0
Simple	0	1	0.9	1.1	-13.04	-12.59	NA	0.08	0.08	3.9
Simple	0	3	0.9	3.1	-13.04	-12.14	0.08	0.04	0.06 ± 0.03	3.9
Simple	0	10	0.9	10.1	-13.04	-11.63	0.31	0.23	0.27 ± 0.06	42.5
Simple	0	30	0.9	30.1	-13.04	-11.15	0.34	0.32	0.33 ± 0.02	54.6
Simple	0	100	0.9	100.1	-13.04	-10.63	0.36	0.34	0.35 ± 0.01	47.1
Matrix	100	100	100.9	100.1	-10.99	-10.63	0.35	0.42	0.39 ± 0.05	43.4
Matrix	30	30	30.9	30.1	-11.50	-11.15	0.38	0.32	0.35 ± 0.04	88.2
Matrix	100	10	100.9	10.1	-10.99	-11.63	0.34	0.36	0.35 ± 0.01	73.8
Matrix	10	100	10.9	100.1	-11.95	-10.63	0.36	0.31	0.34 ± 0.04	91.4
Matrix	30	3	30.9	3.1	-11.50	-12.14	0.11	0.09	0.10 ± 0.01	8.5
Matrix	3	30	3.9	30.1	-12.40	-11.15	0.19	0.20	0.20 ± 0.01	29.7
Matrix	1	100	1.9	100.1	-12.71	-10.63	0.28	0.18	0.20 ± 0.07	79.0
Matrix	100	1	100.9	1.1	-10.99	-12.59	0.38	0.40	0.39 ± 0.01	59.9

Table 5. Growth rates of NE Pacific *Pseudo-nitzschia delicatissima* UNC1205 in Zn and Co simple limitation (one element varies) and matrix (both elements covaried) treatments. Simple limitation was conducted in duplicate (replicates A and B). Metal concentrations are provided as the amount of metal added to each media treatment ("Added [M]" column), the total metal concentration (background media concentration + added concentration, "Total [M]*" column), and the concentration of free metal ions calculated using the total metal concentration and media composition ("log[M^{2+}]" columns). Average growth rates are given ± the standard deviation of duplicate growth rates. NA refers to not available. Biomass yield is reported as relative fluorescent units (RFU).

Experiment Type	Added [Zn] (nM)	Added [Co] (nM)	Total [Zn]* (nM)	Total [Co]* (nM)	$\log[\mathrm{Zn}^{2+}]$ (M)	$\log[\mathrm{Co}^{2+}]$ (M)	Growth rate replicate A	Growth rate replicate B	Growth rate average (d^{-1})	Yield (Maximum RFU)
Simple	0	0	0.9	0.1	-13.04	-13.63	0.09	0.04	0.06 ± 0.04	6.9
Simple	1	0	1.9	0.1	-12.71	-13.63	0.38	0.50	0.44 ± 0.08	16.4
Simple	3	0	3.9	0.1	-12.40	-13.63	0.49	0.53	0.51 ± 0.03	23.7
Simple	10	0	10.9	0.1	-11.95	-13.63	0.61	0.51	0.56 ± 0.07	32.1
Simple	30	0	30.9	0.1	-11.50	-13.63	0.64	0.76	0.70 ± 0.09	105.8
Simple	100	0	100.9	0.1	-10.99	-13.63	0.58	0.64	0.61 ± 0.04	65.2
Simple	0	1	0.9	1.1	-13.04	-12.59	0.26	0.23	0.24 ± 0.02	51.6
Simple	0	3	0.9	3.1	-13.04	-12.14	0.59	0.54	0.56 ± 0.04	99.0
Simple	0	10	0.9	10.1	-13.04	-11.63	0.60	0.68	0.64 ± 0.06	54.8
Simple	0	30	0.9	30.1	-13.04	-11.15	0.68	0.56	0.62 ± 0.08	84.6
Simple	0	100	0.9	100.1	-13.04	-10.63	0.74	0.76	0.75 ± 0.02	110.2
Matrix	100	100	100.9	100.1	-10.99	-10.63	0.86	0.87	0.86 ± 0.01	223.2
Matrix	10	10	10.9	10.1	-11.95	-11.63	0.89	0.94	0.92 ± 0.03	226.6
Matrix	30	30	30.9	30.1	-11.50	-11.15	0.94	0.97	0.96 ± 0.02	234.5
Matrix	100	10	100.9	10.1	-10.99	-11.63	0.93	0.96	0.95 ± 0.02	211.6
Matrix	10	100	10.9	100.1	-11.95	-10.63	0.87	0.92	0.90 ± 0.04	203.5
Matrix	30	3	30.9	3.1	-11.50	-12.14	0.84	0.93	0.88 ± 0.06	209.3
Matrix	3	30	3.9	30.1	-12.40	-11.15	0.88	0.83	0.86 ± 0.03	186.5
Matrix	1	100	1.9	100.1	-12.71	-10.63	0.92	0.83	0.87 ± 0.06	195.6
Matrix	100	1	100.9	1.1	-10.99	-12.59	0.94	0.93	0.94 ± 0.003	233.8

Table 6. Maximum growth rates (μ_{Max}) and half saturation constants (K_m) observed in Zn and Co simple limitation experiments for each diatom strain. μ_{Max} and K_m values were calculated for simple limitation experiment growth rates where curve fitting was applicable. NA refers to not applicable.

Diatom	μ_{MaxCo} (d^{-1})	μ_{MaxZn} (d^{-1})	K_{mCo} ([M^{2+}], mol L^{-1})	K_{mZn} ([M^{2+}], mol L^{-1})	μ_{MaxCo} / μ_{MaxZn}	K_{mCo} / K_{mZn}
Thalassiosira pseudonana CCMP1335	0.39	0.79	3.09×10^{-13} $(r^2 = 0.98)$	5.11×10^{-13} $(r^2 = 0.94)$	0.49	0.60
Phaeodactylum tricornutum CCMP632	0.67	0.79	NA	3.20×10^{-14} $(r^2 = 0.88)$	0.85	NA
Thalassiosira UNC1203	0.39	0.30†	1.62×10^{-12} $(r^2 = 0.94)$	NA	1.3	NA
Pseudo-nitzschia delicatissima UNC1205	0.72	0.69	3.56×10^{-13} $(r^2 = 0.95)$	1.96×10^{-13} $(r^2 = 0.83)$	1.04	1.82

† μ_{MaxZn} for *Thalassiosira* UNC1203 cannot be determined by Monod curve fitting and is instead taken as the observed maximum growth rate achieved under simple Zn limitation.

Table 7. Cobalt, zinc, and cadmium cellular metal quotas and uptake rates (ρ) measured in selected matrix experiment cultures of NE Pacific *P. delicatissima*, NE Pacific *Thalassiosira* UNC1203, and Atlantic *P. tricornutum*. Cellular metal quotas are normalized to cellular P. For all samples, $Co^{2+} = 23.4$ pM. BD refers to below detection. NA refers to not applicable.

Diatom	Total Zn (nM)	Total Co (nM)	Growth rate average (d^{-1})	Co:P (mmol mol^{-1})	Zn:P (mmol mol^{-1})	Cd:P (µmol mol^{-1})	ρCo (mmol mol P^{-1} d^{-1})	ρZn (mmol mol P^{-1} d^{-1})	ρCd (µmol mol P^{-1} d^{-1})
P. delicatissima	1.9	100.1	0.87	0.44	0.16	0.13	0.38	0.14	0.11
	10.9	100.1	0.90	0.26	0.37	0.15	0.23	0.33	0.14
	100.9	100.1	0.86	0.08	0.45	0.07	0.07	0.39	0.06
Thalassiosira UNC1203	1.9	100.1	0.20	0.40	BD	0.22	0.08	NA	0.04
	10.9	100.1	0.34	0.33	0.01	0.14	0.11	0.003	0.05
	100.9	100.1	0.39	0.21	0.09	0.13	0.08	0.04	0.05
P. tricornutum	1.9	100.1	0.79	0.02	0.01	0.17	0.02	0.01	0.13
	10.9	100.1	0.77	0.01	0.75	0.18	0.01	0.58	0.14
	100.9	100.1	0.90	0.01	2.36	0.02	0.01	2.12	0.02

56

Figures

a.

b.

c.

d.

e.

57
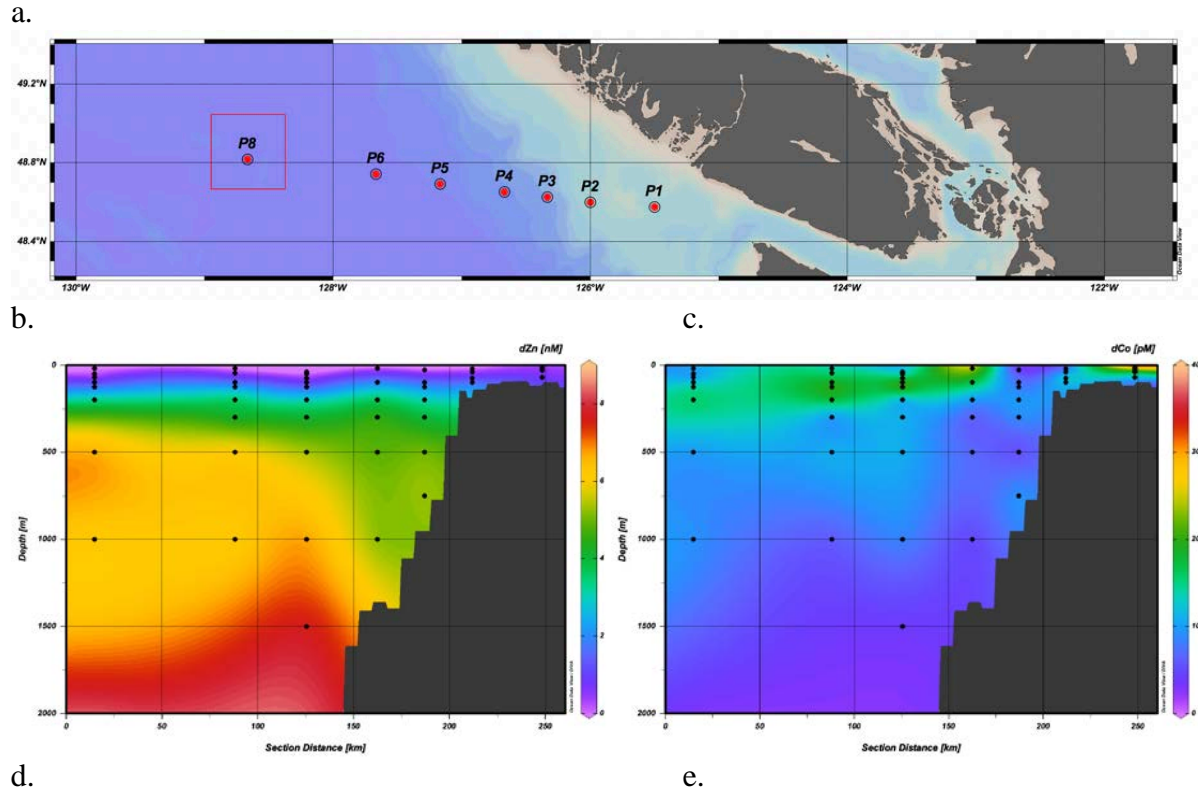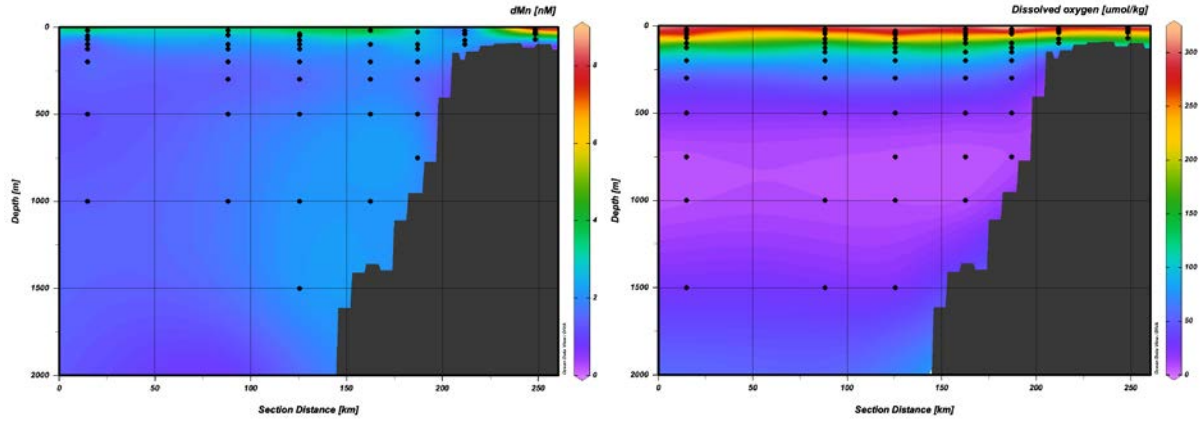
Figure 1. Location of the Line P transect and dissolved metal data. (a) Stations sampled on cruise TN280 from 17-22 May 2012. Station numbers are the same as those used by the Line P program. *Thalassiosira* UNC1203 and *Pseudo-nitzschia delicatissima* UNC1205 used in this study were isolated from station P8 (red box). The concentration of total dissolved Zn (b), total dissolved Co (c), total dissolved Mn (d), and dissolved oxygen (e) in color scale along the transect.

a.

b.

58
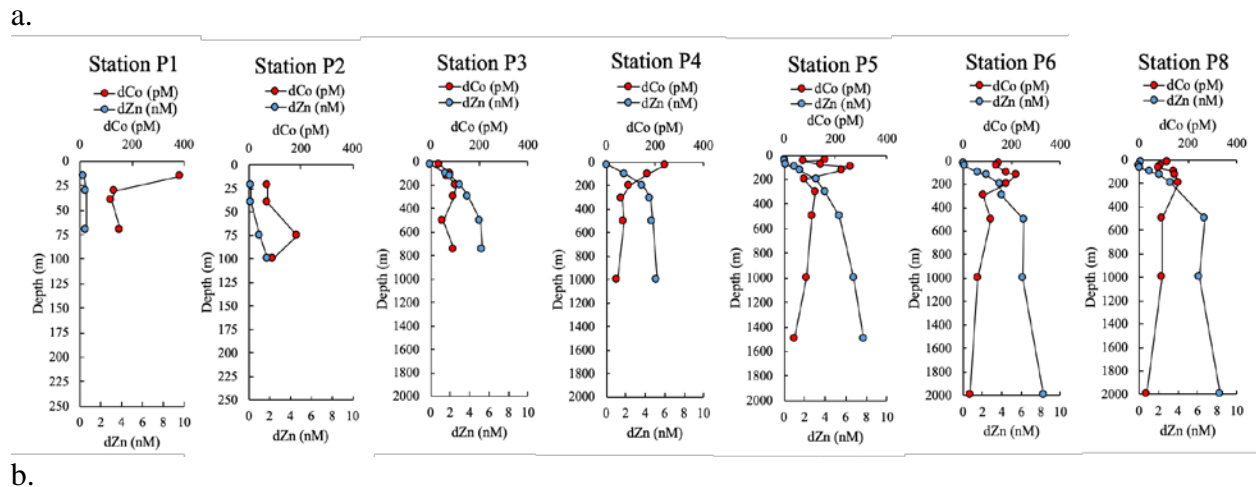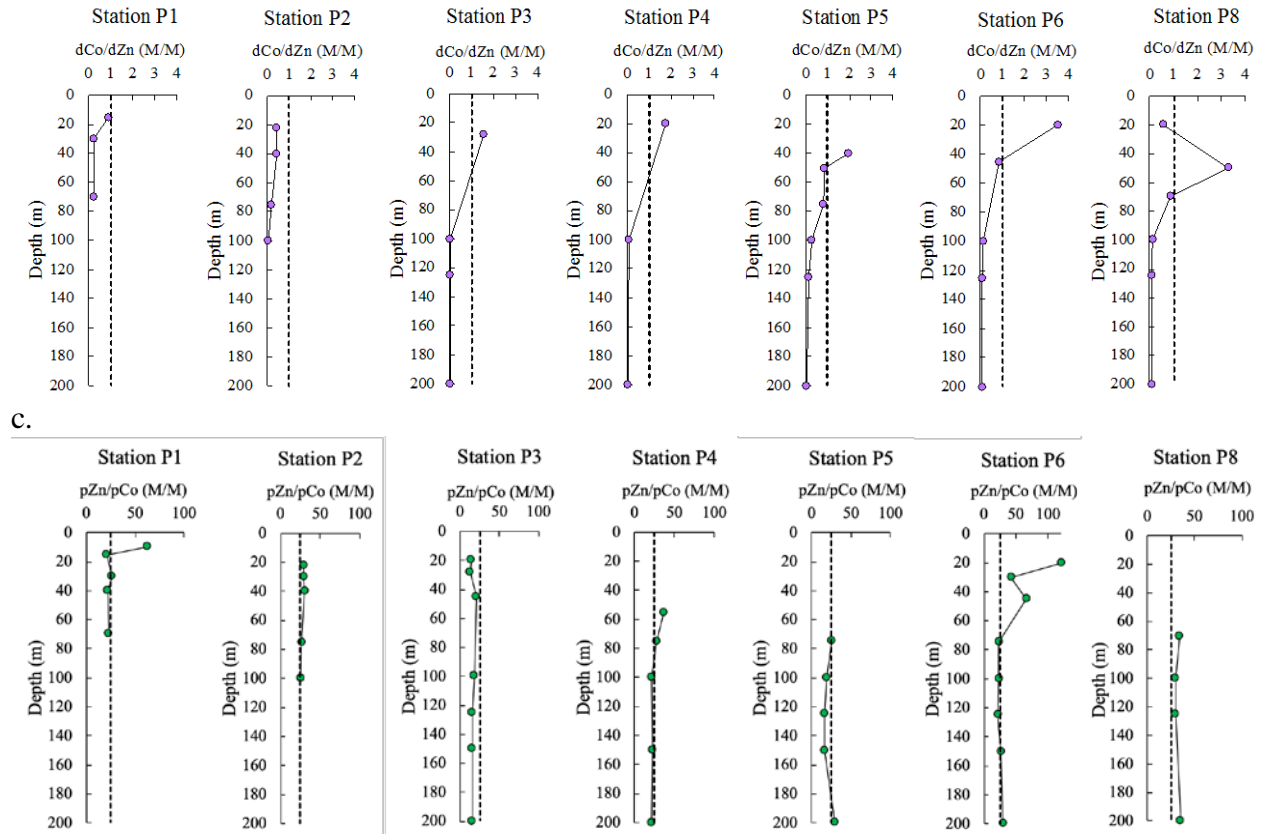
Figure 2. Total dissolved depth profiles, total dissolved molar ratios, and total particulate molar ratios of Co and Zn along the transect. (a) Depth profiles of dCo and dZn at stations P1 – P8. Note that for the coastal stations P1 and P2, depth profiles are scaled to 250m max depth. (b) Surface (0 – 200 m) molar ratios of dCo:dZn at each station. The vertical dashed line denotes a dCo:dZn ratio of 1:1. (c) Surface molar ratios of pZn:pCo at each station. The vertical dashed line denotes a pZn:pCo ratio of 25:1.

a.   b.
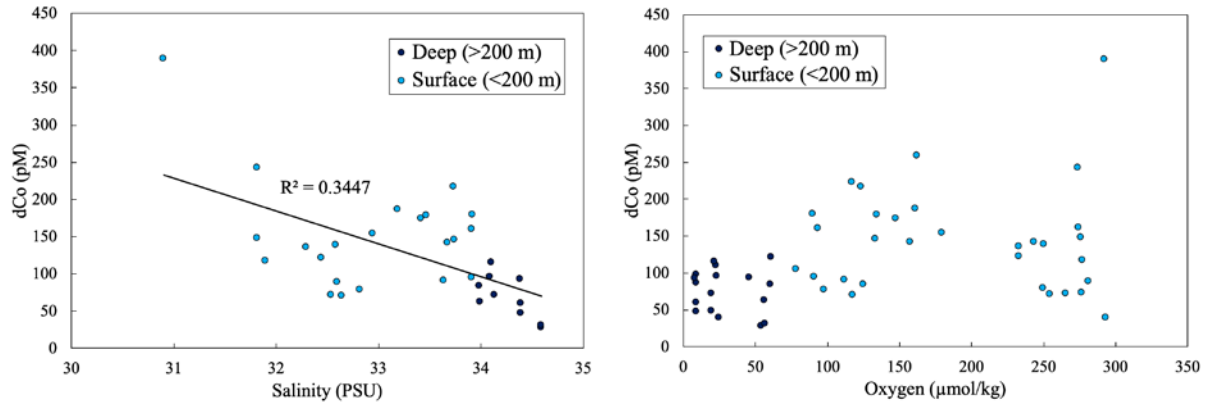
Figure 3. Relationships between total dissolved Co and other measured parameters along the transect. (a) A weak correlation between dCo and salinity may imply a freshwater source of dCo input. (b) dCo and dissolved oxygen share no correlation.
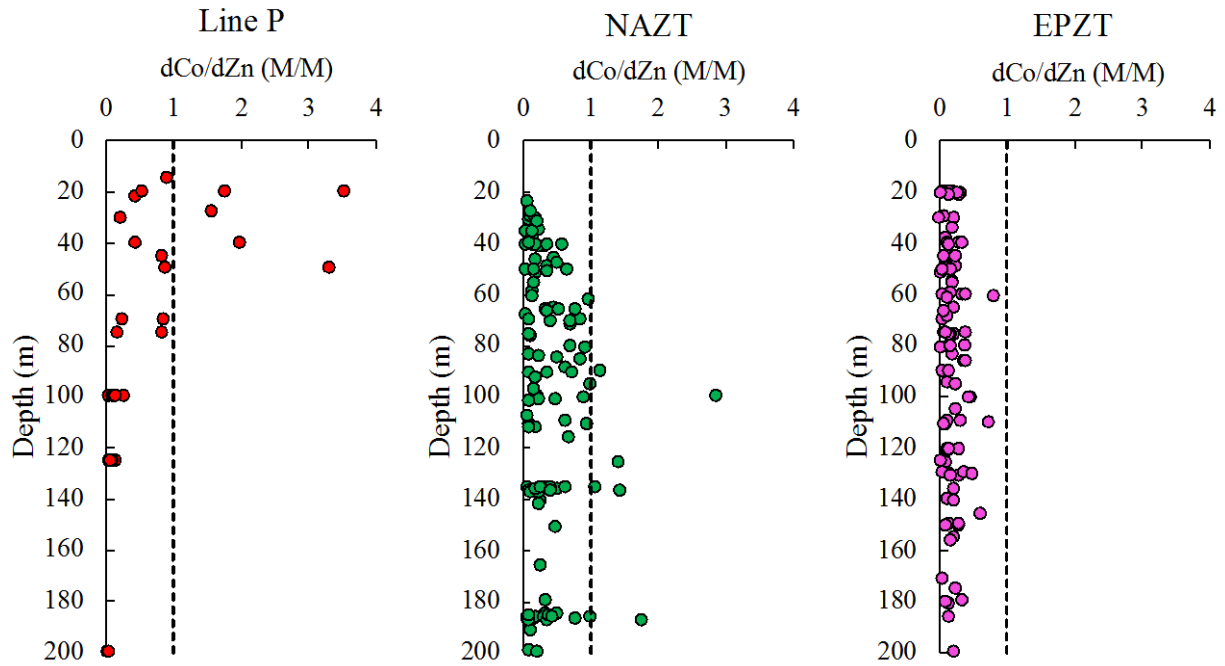
Figure 4. Comparison of Line P, NAZT, and EPZT dCo:dZn ratios for all stations and depths. NAZT data was collected as part of the GEOTRACES Eastern North Atlantic cruise from Lisbon to Cape Verde (October 2010, cruise KN199-04) and Western North Atlantic cruise from Woods Hole MA, USA to Bermuda (December 2011, KN204-01A). EPZT data was collected as part of the GEOTRACES Eastern Pacific Zonal Transect (EPZT) cruise from Peru to Tahiti (October 2013, cruise TGT303). The vertical dashed line denotes a dCo:dZn ratio of 1:1.

61
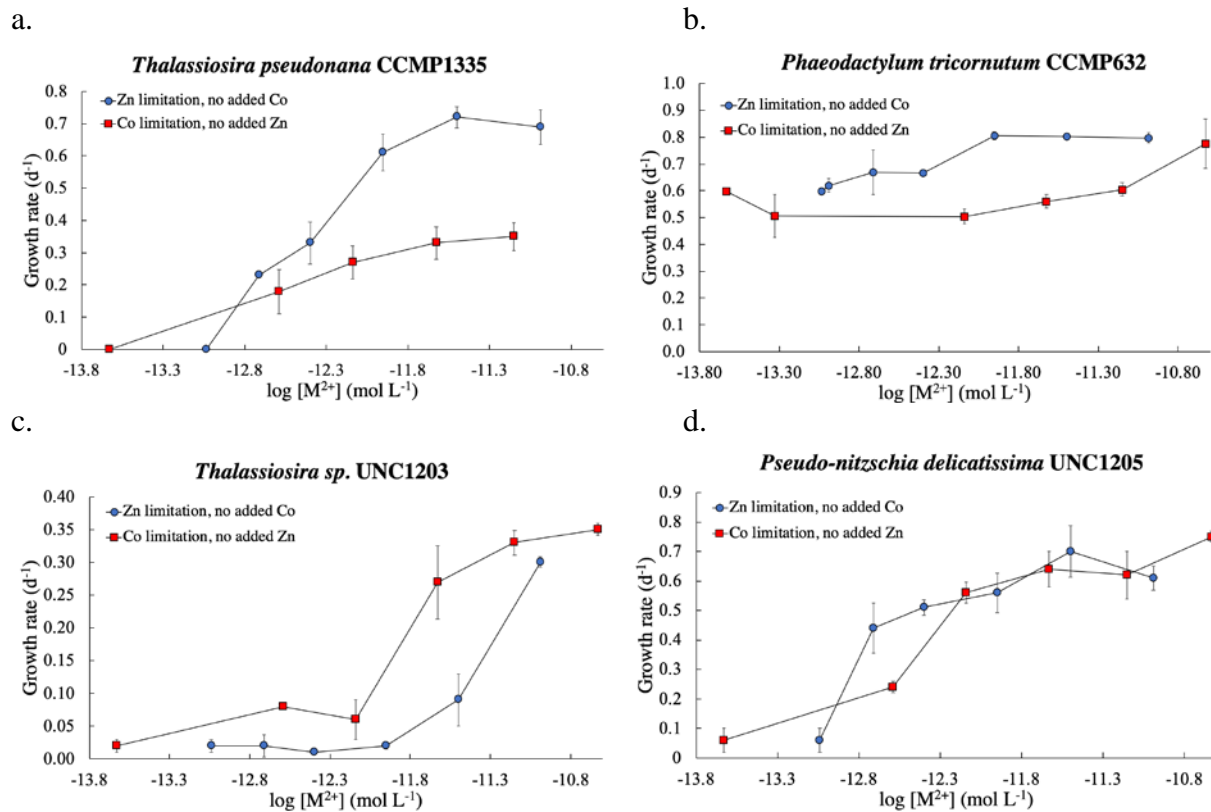
Figure 5. Growth rates of the Atlantic isolates (a) *Thalassiosira pseudonana* and (b) *Phaeodactylum tricornutum* and of the NE Pacific isolates (c) *Thalassiosira* UNC1203 and (d) *Pseudo-nitzschia delicatissima* in varying zinc concentrations with no added cobalt (Zn limitation, no Co) and varying cobalt concentrations with no added zinc (Co limitation, no Zn). Error bars are calculated using the standard deviation of biological duplicates.
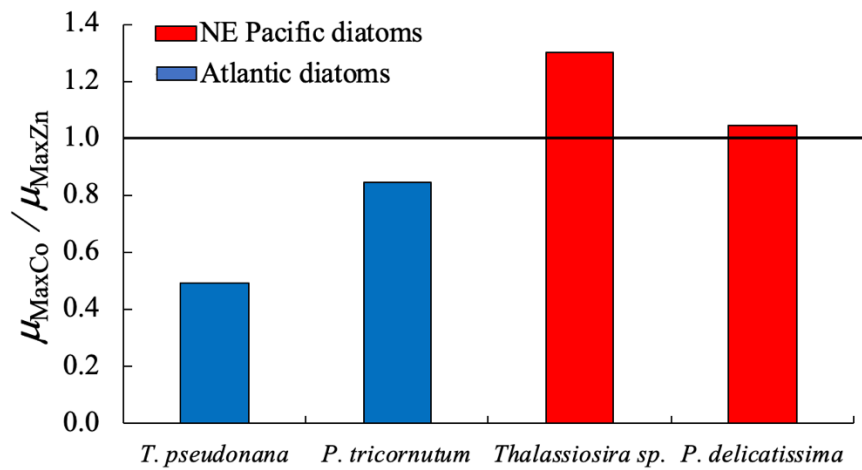
Figure 6. Ratios of maximum growth rates in cobalt (μ_{MaxCo}) to maximum growth rates in zinc (μ_{MaxZn}) observed in Zn and Co simple limitation experiments for all diatom strains. Data plotted from Table 6.

63

a.   b.
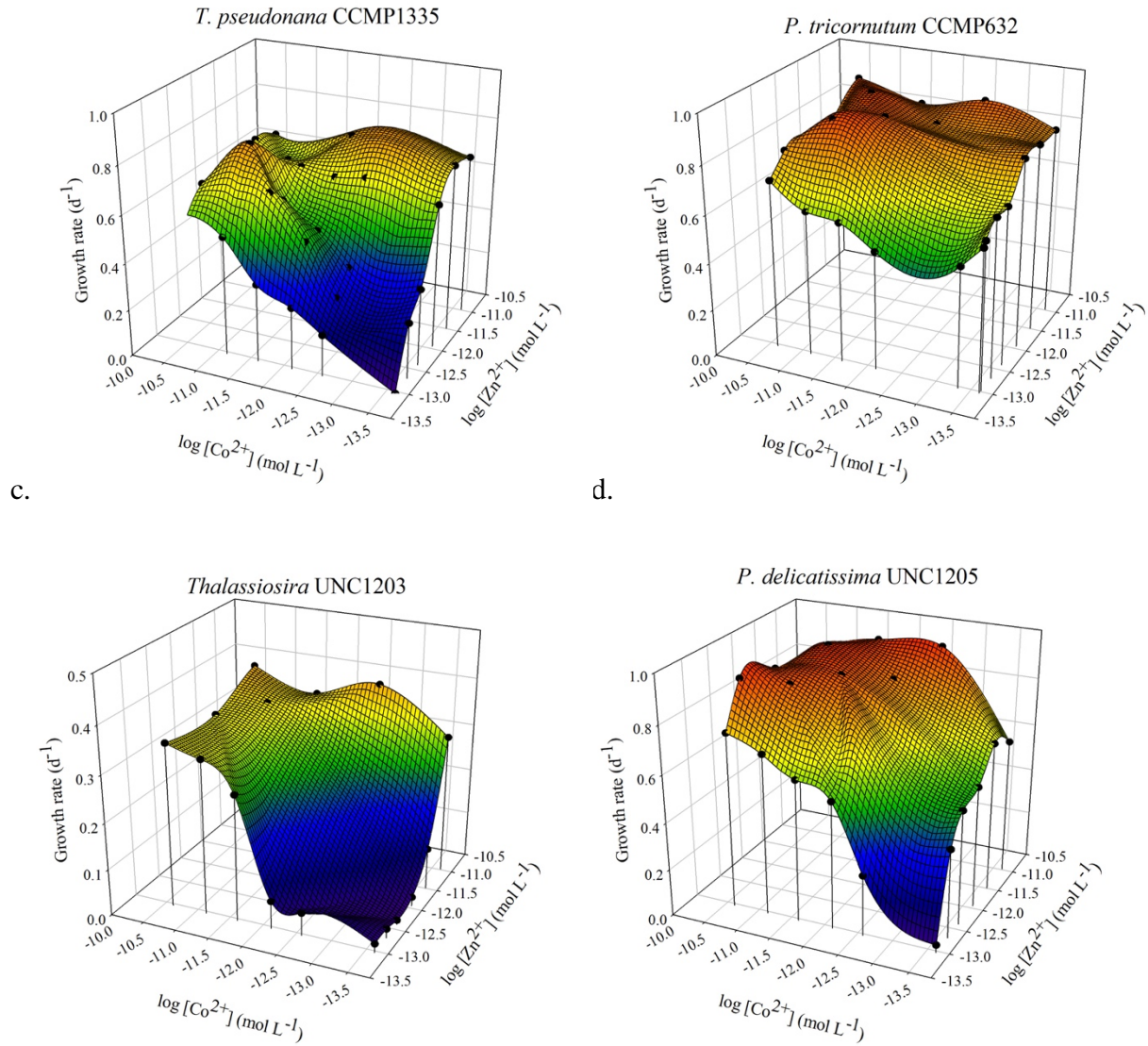
Figure 7. Growth rates of (a) *T. pseudonana,* (b) *P. tricornutum*, (c) *Thalassiosira sp.,* and (d) *P. delicatissima* in covarying cobalt and zinc concentrations. Growth rates from both simple limitation and matrix experiments (Tables 2-5) were averaged to generate the surface mesh, while individual data points are overlaid (black circles). Growth rates from simple limitation cultures are denoted by drop pins. Note the shorter z-axis scale for *Thalassiosira* UNC1203.

a.

P. tricornutum CCMP632

b.

P. tricornutum CCMP632

c.

Thalassiosira UNC1203

d.

P. delicatissima UNC1205
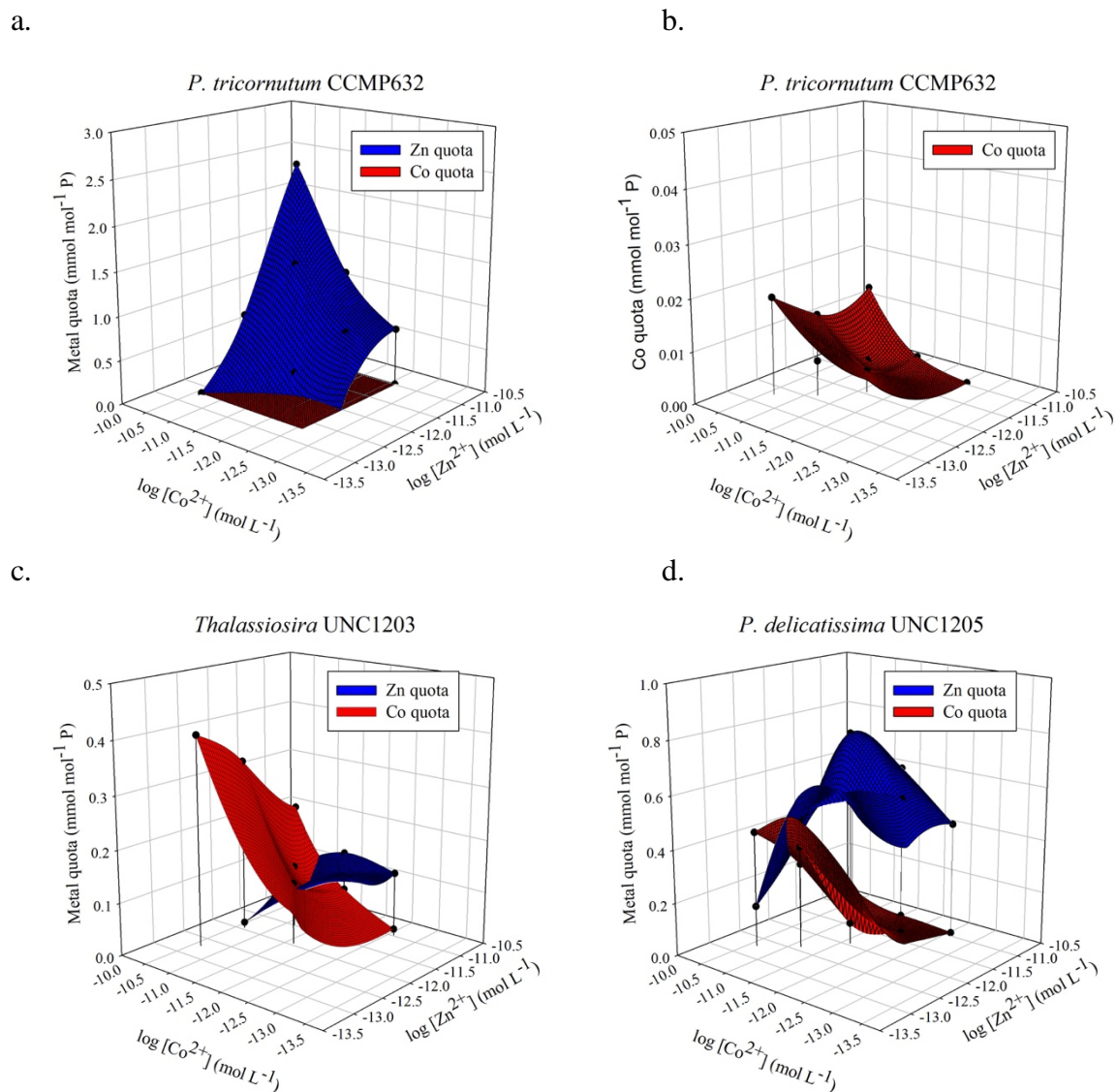
Figure 8. Cellular Zn and Co quotas of matrix cultures of the Atlantic diatom *P. tricornutum* (a,b) and of the NE Pacific diatoms *Thalassiosira* UNC1203 (c) and *P. delicatissima* UNC1205 (d). Cellular metal concentrations are normalized to cellular P concentrations. Metal quotas from matrix experiment cultures were averaged to generate the surface mesh, while individual data

66

points are overlaid (black circles with drop pins). Co:P quotas in *P. tricornutum* are plotted separately in (b) to show the trend of decreasing Co:P quotas with increasing Zn^{2+}.
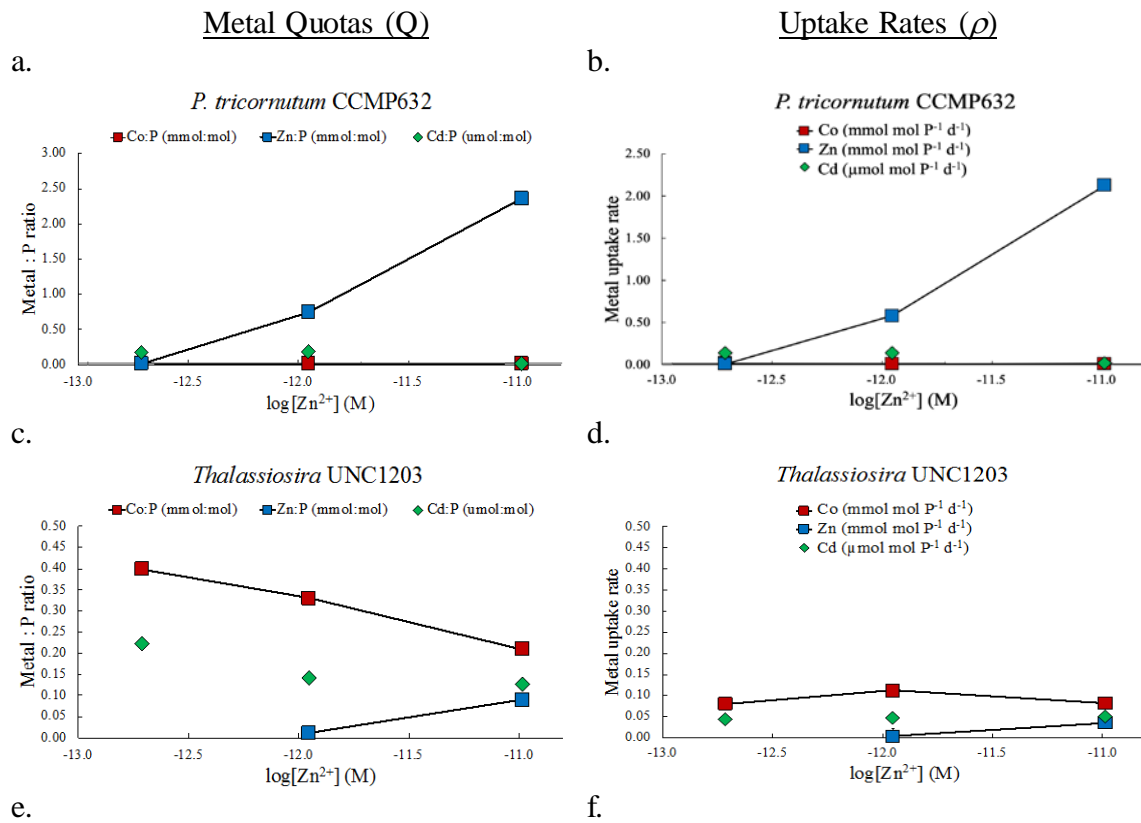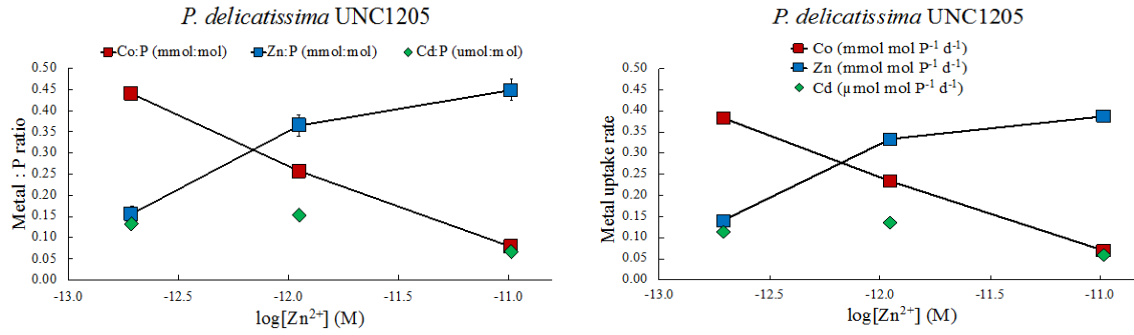
Figure 9. Cellular Zn, Co, and Cd quotas and uptake rates for selected matrix cultures of Atlantic *P. tricornutum* CCMP632 (a,b), NE Pacific *Thalassiosira* UNC1203 (c,d), and NE Pacific *P. delicatissima* UNC1205 (e,f). Cellular metal quotas are normalized to cellular P. For all samples, $Co^{2+} = 23.4$ pM. Data plotted from Table 7. Error bars are the standard deviation of technical duplicates.

a.

b.

Co:C

c.

Co:Zn
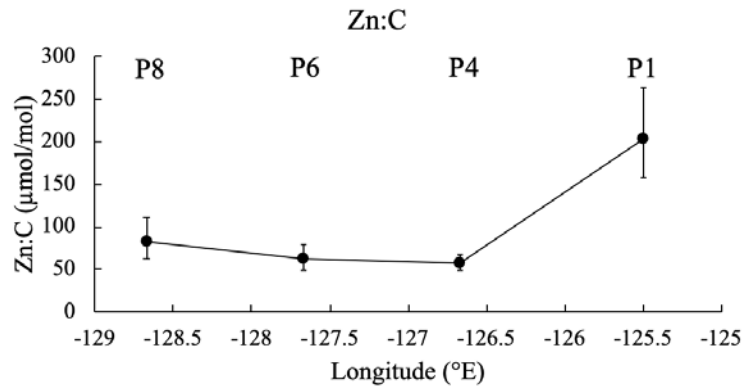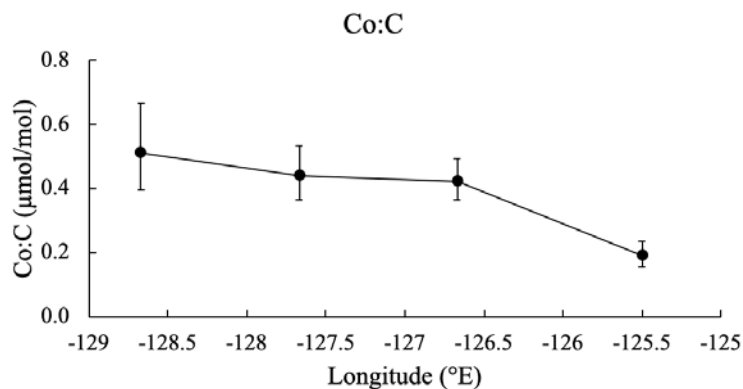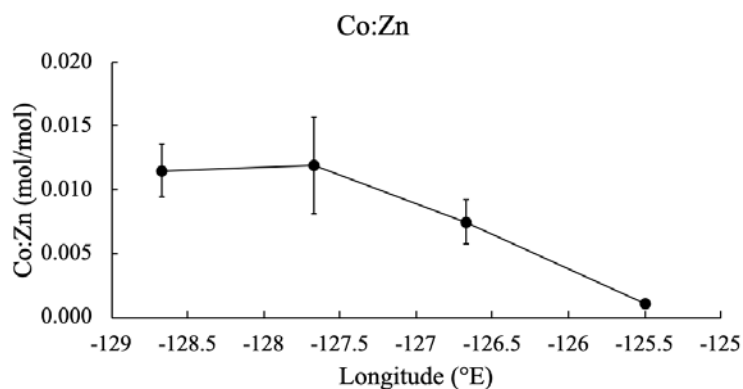
Figure 10. Metal contents of individual cells sampled from stations P1, P4, P6 and P8 of the Line P transect analyzed by synchrotron X-ray fluorescence (SXRF). Geometric mean values of 10-15 cells analyzed per station are plotted ± the standard error. (a) Cellular Zn content normalized to cellular C. (b) Cellular Co content normalized to cellular C. (c) Ratios of cellular Co:Zn.
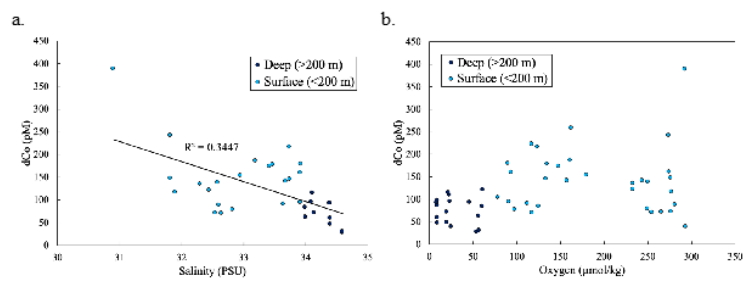
a.

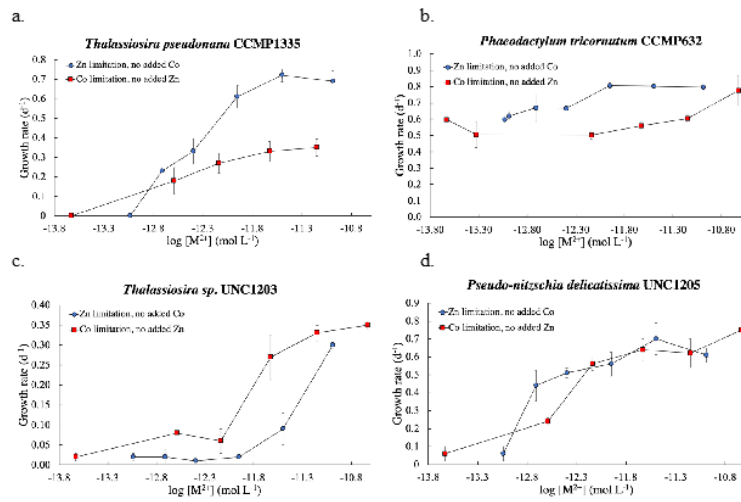69

Mn Cell Quotas
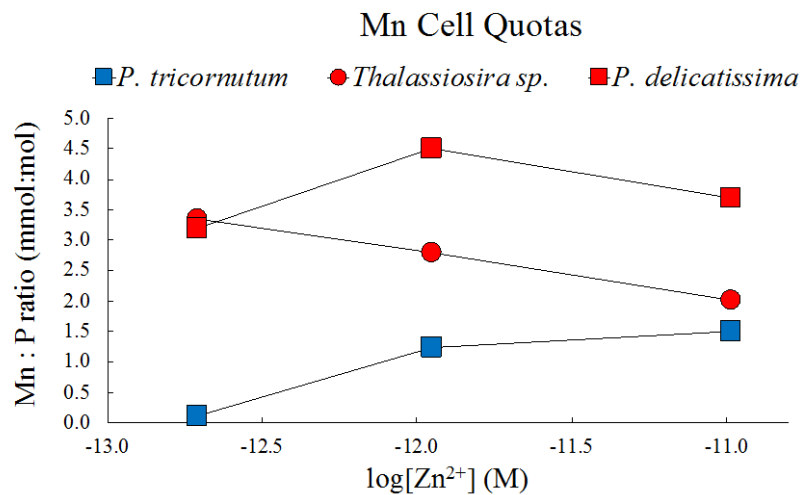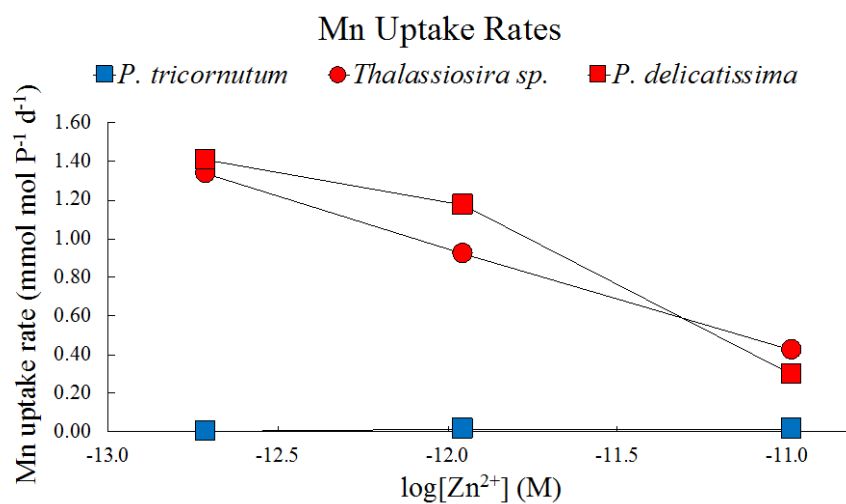
Mn Uptake Rates

Figure 11. Cellular Mn quotas (a) and uptake rates (b) for selected matrix cultures of Atlantic *P. tricornutum* CCMP632 and of the NE Pacific diatoms *Thalassiosira* UNC1203 and *P. delicatissima* UNC1205. Cellular metal quotas are normalized to cellular P. For all samples, Co^{2+} = 23.4 pM.
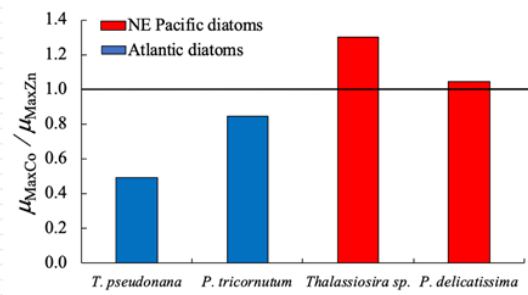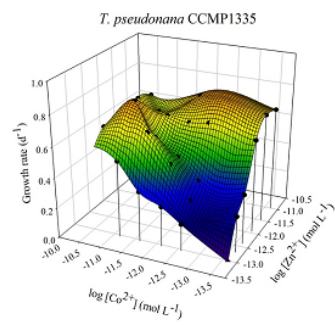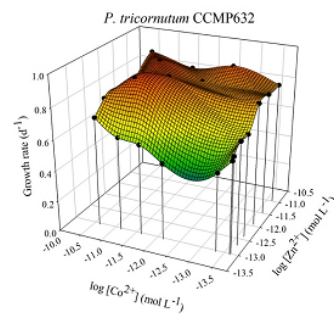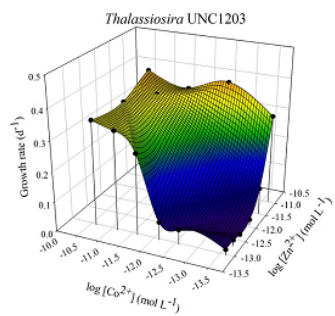
a.

b.

dZn [nM]

c.

dCo [pM]

d.

dMn [nM]

e.

Dissolved oxygen [umol/kg]

a.

Station P1

dCo (pM)

Station P2

dCo (pM)

Station P3

dCo (pM)

Station P4

dCo (pM)

Station P5

dCo (pM)

Station P6

dCo (pM)

Station P8

dCo (pM)

b.

Station P1

dCo/dZn (M/M)

Station P2

dCo/dZn (M/M)

Station P3

dCo/dZn (M/M)

Station P4

dCo/dZn (M/M)

Station P5

dCo/dZn (M/M)

Station P6

dCo/dZn (M/M)

Station P8

dCo/dZn (M/M)

c.

Station P1

pZn/pCo (M/M)

Station P2

pZn/pCo (M/M)

Station P3

pZn/pCo (M/M)

Station P4

pZn/pCo (M/M)

Station P5

pZn/pCo (M/M)

Station P6

pZn/pCo (M/M)

Station P8

pZn/pCo (M/M)

a.

b.

Line P
dCo/dZn (M/M)

NAZT
dCo/dZn (M/M)

EPZT
dCo/dZn (M/M)

a.

T. pseudonana CCMP1335

b.

P. tricornutum CCMP632

c.

Thalassiosira UNC1203

d.

P. delicatissima UNC1205

a.

P. tricornutum CCMP632

b.

P. tricornutum CCMP632

c.

Thalassiosira UNC1203

d.

P. delicatissima UNC1205

Metal Quotas (Q)   Uptake Rates (ρ)

a.

P. tricornutum CCMP632

■ Co:P (mmol:mol)   ■ Zn:P (mmol:mol)   ◆ Cd:P (umol:mol)

b.

P. tricornutum CCMP632

■ Co (mmol mol P⁻¹ d⁻¹)
■ Zn (mmol mol P⁻¹ d⁻¹)
◆ Cd (μmol mol P⁻¹ d⁻¹)

c.

Thalassiosira UNC1203

■ Co:P (mmol:mol)   ■ Zn:P (mmol:mol)   ◆ Cd:P (umol:mol)

d.

Thalassiosira UNC1203

■ Co (mmol mol P⁻¹ d⁻¹)
■ Zn (mmol mol P⁻¹ d⁻¹)
◆ Cd (μmol mol P⁻¹ d⁻¹)

e.

P. delicatissima UNC1205

■ Co:P (mmol:mol)   ■ Zn:P (mmol:mol)   ◆ Cd:P (umol:mol)

f.

P. delicatissima UNC1205

■ Co (mmol mol P⁻¹ d⁻¹)
■ Zn (mmol mol P⁻¹ d⁻¹)
◆ Cd (μmol mol P⁻¹ d⁻¹)

a.

Zn:C

b.

Co:C

c.

Co:Zn

a.

b.